 ISSN 0267-8179. DOI: 10.1002/jqs.2976

JQS Journal of Quaternary Science QRA Quaternary Research Association

Stratigraphy, age and correlation of Lepué Tephra: a widespread *c.* 11 000 cal a BP marker horizon sourced from the Chaitén Sector of southern Chile

BRENT V. ALLOWAY,[1,2]* PATRICIO I. MORENO,[3] NICK J. G. PEARCE,[4] RICARDO DE POL-HOLZ,[5] WILLIAM I. HENRÍQUEZ,[6] OSCAR H. PESCE,[3] ESTEBAN SAGREDO,[7] GUSTAVO VILLAROSA[8] and VALERIA OUTES[8]

[1]School of Environment, University of Auckland, Auckland, New Zealand
[2]Centre for Archaeological Science (CAS), School of Earth and Environmental Sciences, University of Wollongong, Wollongong, NSW, Australia
[3]Departamento de Ciencias Ecológicas, Instituto de Ecología y Biodiversidad, Universidad de Chile, Santiago, Chile
[4]Department of Geography & Earth Sciences, Aberystwyth University, Wales, UK
[5]GAIA-Antártica, Universidad de Magallanes, Punta Arenas, Chile
[6]School of Geography, Environment and Earth Sciences, Victoria University of Wellington, Wellington, New Zealand
[7]Instituto de Geografía, Pontificia Universidad Católica de Chile, Santiago, Chile
[8]IPATEC, CONICET-Universidad Nacional del Comahue, Bariloche, Argentina

Received 13 November 2016; Revised 23 May 2017; Accepted 24 May 2017

ABSTRACT: We describe the stratigraphy, age and correlation of a prominent tephra marker, named Lepué Tephra, extensively distributed in north-western Patagonia. Lepué Tephra is well dated at *c.* 11 000 cal a BP from numerous lake and soil cover-bed sequences and its recognition is useful for assessing the rate and timing of deglaciation as well as associated environmental changes in this region during the last glacial termination and early Holocene. Lepué Tephra has attributes typical of a complex and compositionally zoned phreatomagmatic eruptive. While the initial rhyolitic phase can be readily distinguished from multiple eruptive products sourced from the adjacent Volcán Chaitén, the main erupted end member is of basaltic–andesitic bulk composition – similar to younger tephras sourced from Holocene monogenetic cones adjacent to the Volcán Michimahuida massif (tMim). Lepué Tephra can be correlated to an equivalent-aged pyroclastic flow deposit (Amarillo Ignimbrite) prominently distributed in the south-eastern sector of tMim. The source vent for these co-eruptive events is obscured by an extensive ice field and is currently unknown. The widespread radially symmetrical distribution of Lepué Tephra centred on tMim cannot be attributed solely to volcanological considerations. Reduced Southern Hemisphere westerly wind influence interpreted from climate proxies at the time of eruption are also implicated.
Copyright © 2017 John Wiley & Sons, Ltd.

KEYWORDS: Lepué Tephra; north-west Patagonia; tephrostratigraphy; Volcán Chaitén; Volcán Michimahuida.

Introduction

The ability to recognize, correlate and characterize tephra of mafic to intermediate–silicic compositions that have been subjected to intense post-depositional weathering and disturbance in temperate to tropical climate environments is a significant obstacle to tephra studies in many proximal to distal volcanic settings. Not only does the intense post-depositional pedogenic weathering effectively mask fine-grained and/or thin tephra inter-beds within soil-dominated cover-beds, it potentially compromises the morphological expression of the tephra as well as its constituent geochemistry and grain-size characteristics – all attributes of which are fundamental in tephra correlation. The characterization of such tephra already susceptible to post-depositional alteration can be further complicated by compositional heterogeneity – that is, upward changes in tephra composition as an eruption progresses. Such changes may reflect sequential surface discharge of either a compositionally segregated magma body in the sub-volcanic system or a sudden magmatic recharge event into an already fractionating body.

The principal objective of this study is to describe the stratigraphy, distribution, age and geochemistry of a prominent tephra marker (here formally named Lepué Tephra) located in the hyper-humid and high-weathering andic environment of north-western Patagonia (Fig. 1). The stratigraphy, age and chemistry of associated rhyolitic tephra sourced from Volcán Chaitén will be presented in a companion paper (see Alloway *et al.*, 2017). Lepué Tephra is regionally important for three reasons. First, it is one of the most widespread tephra marker beds to occur in this sector and is therefore ideal for assessing the timing and rate of deglaciation and associated environmental changes in this region during the Pleistocene–Holocene transition. Second, Lepué Tephra can be recognized in high-resolution lacustrine and marine records and is therefore an important isochron potentially useful in assessing proxy record synchroneity between equivalent-aged offshore and onshore sequences. Third, Lepué Tephra is difficult to characterize chemically because of the ubiquitous occurrence of microphenocrysts and compositional heterogeneity of glassy constituents. Hence, the application of a combination of grain discrete and bulk major and trace elemental techniques may be a useful template by which other similarly difficult tephra might be characterized, Finally, Lepué Tephra provides a unique insight into a compositionally zoned and complex phreatomagmatic eruption associated with a permanent Andean ice cap.

*Correspondence to: B. V. Alloway, as above.
E-mail: brent.alloway@gmail.com

Copyright © 2017 John Wiley & Sons, Ltd.

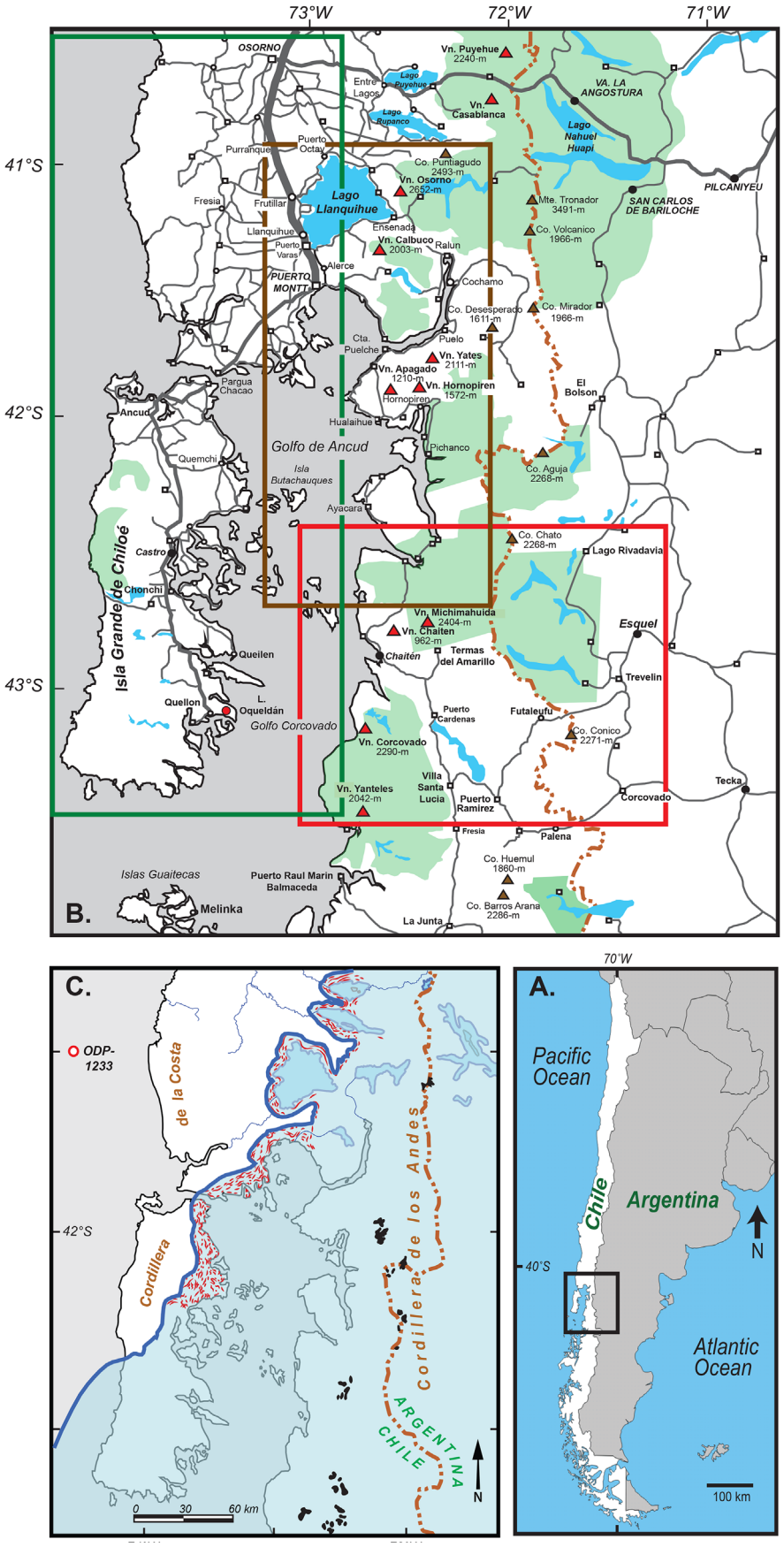

Figure 1. (A, B) The location of the study area in Llanquihue-Puerto Montt, Hornopirén, Chaitén, Isla Grande de Chiloé and Esquel sectors of north-western Patagonia. Coloured insets within B indicate the location of key transects presented in this paper that detail the stratigraphy of Lepué Tephra. (C) Extent of ice lobes within the study area during the Last Glacial Maximum (LGM) (modified from plates 1–4 *in* Denton *et al.*, 1999). Moraine ridges or hills are indicated in red and areas of present-day permanent ice are indicated in black. The location of core ODP Site 1233 offshore of southern continental Chile is also indicated.

Copyright © 2017 John Wiley & Sons, Ltd.

Setting

North-western Patagonia encompasses the Chilean Lake District and Chilotan Archipelago (40–44°S), and is bounded in the east by the Andes Cordillera and a lower lying coastal range in the west adjacent to the Pacific Ocean (Fig. 1). This region frequently experiences intermittent eruptions of varying magnitude from compositionally diverse volcanoes situated within the Andean Southern Volcanic Zone (SVZ). At least 60 active or potentially active volcanoes in Chile and Argentina, as well as three caldera systems and numerous minor eruptive centres (Stern, 2004; Stern *et al.*, 2007) occur within this zone. Volcanism results from the subduction of the Nazca Plate beneath the westward moving South American Plate (Stern, 2004), along a narrow volcanic arc that follows the Liquiñe–Ofqui fault system in Chile between 33 and 46°S. Several volcanoes within this zone have recently erupted – the most notable being Volcán Chaitén (VCha) in 2008, Puyehue-Cordon Caulle in 2011 and Calbuco in 2015.

Over the last two decades, a number of studies have detailed the late last glacial to Holocene tephrostratigraphy of north-western Patagonia to develop an inventory of eruptive events, determine source as well as characterize size, composition and timing (i.e. Naranjo and Stern, 2004; Stern, 2008). While some eruptive histories of individual volcanic centres within the central portions of the SVZ have been described in detail (Lara *et al.*, 2006; Singer *et al.*, 2008), the eruptive histories of many centers particularly within the southern SVZ (SSVZ) are insufficiently known owing to their remote locations and inaccessibility (Watt *et al.*, 2011). Tephra layers have been routinely recorded in lakes (i.e. Haberle and Lumley, 1998; Daga *et al.*, 2010; Moreno *et al.*, 2015a) but in many studies the occurrence of tephra has been a subordinate focus in dominantly paleoecologically and paleoclimatically directed investigations (i.e. Abarzúa *et al.*, 2004; Bertrand *et al.*, 2008; Iglesias *et al.*, 2012; Moreno and Videla, 2016). The need to better utilize tephra within sedimentary archives as an effective means to synchronize records was recently highlighted by Fontijn *et al.* (2016). Recent research efforts has also tended to focus on examining composite eruptive records to better assess region-wide hazards based on magnitude/frequency of historical and prehistoric eruptive events across large swaths of Patagonia (i.e. Stern, 2008; Watt *et al.*, 2011; Fontijn *et al.*, 2014; Rawson *et al.*, 2015; Naranjo *et al.*, 2017). Recent eruptions (i.e. Hudson in 1991, Chaitén in 2008, Puyehue Cordón-Caulle in 2011, Calbuco in 2015) have also served as a driver for renewed field investigations so that eruptive histories and potential hazards posed to adjacent and downwind communities can be better clarified (i.e. Lara, 2009; Wilson *et al.*, 2011a, 2011b; Amigo *et al.*, 2013; Lara *et al.*, 2013; Watt *et al.*, 2013; Alloway *et al.*, 2015, 2017).

Another dominant landscape feature is ubiquitous glacial landforms and ice-carved lake basins formed from Andean piedmont glaciers during episodes of cold (glacial) and/or temperate climate through the Quaternary. The configuration of these Andean piedmont ice lobes in north-western Patagonia is well known largely based on the glacial morphological mapping of moraines and outwash plains adjacent to lakes and ocean alongside the western margin of the Andes (Andersen *et al.*, 1999; Denton *et al.*, 1999). These seminal maps not only demarcated moraines and outwash plains deposited during the maximum phases of the last glaciation (locally referred to as Llanquihue glaciation) but also displayed older Casma and Colegual moraines and outwash plains first described by Mercer (1976). Radiocarbon dating of Llanquihue landforms show that the Andean ice lobes advanced into the moraine belt depicted in red in Fig. 1C numerous times during glacial and/or cool interstadial phases of Marine Isotope Stage (MIS) 4, 3 and 2, rather than simply being formed during the Last Glacial Maximum (LGM) in MIS 2. The chronology of the youngest advance is constrained by an extensive array of radiocarbon dates from sites tied to the former Llanquihue, Reloncaví, Ancud and Golfo de Corcovado ice lobes (Denton *et al.*, 1999; Moreno *et al.*, 2015b). Overall this chronology shows a culmination of the glacial readvance at 17 800 cal a BP. The advance of the two northern lobes (Llanquihue and Reloncaví) reached the inner margin of the LGM moraine belt, whereas that of the two southern lobes (Ancud and Golfo de Corcovado) was either the most extensive, or close to the most extensive, of MIS 2.

Of particular relevance to this study are sites located in areas formerly occupied by ice lobes that overlie glacial deposits and contain the Lepué Tephra, as they can assist in constraining the recessional chronology of ice lobes as climate warmed abruptly during the Last Glacial Termination (LGT) (Moreno *et al.*, 2015b).

Stratigraphy

In sections directly adjacent to the Volcán Michimahuida massif (tMim), Lepué Tephra is typically characterized by compact, dark gray to brownish gray, poorly sorted, massive to weakly stratified, scoriaceous lapilli to lapilli-'tuff' (consolidated ash, Fisher and Schmincke, 1984) beds often containing accretionary lapilli. These textural and sorting characteristics, together with highly variable depositional architecture between adjacent sections, suggest 'molten fuel-coolant interactions' (Zimanowski, 1998) resulting in a complex succession of magmatic and phreatomagmatic eruptive products (e.g. Cas and Wright, 1987; Ort and Carrasco-Núñez, 2009; Ngwa *et al.*, 2010; van Otterloo and Cas, 2016).

Proximal

Within sections near Chaitén and Santa Barbara and those sections further north towards Caleta Gonzalo (Fig. 2), a prominent decimeter (dm)-thick reddish brown crudely stratified medium to coarse scoriaceous fall unit is directly overlain by a compact, dm-thick brownish gray, crudely stratified, very poorly sorted ash with conspicuous dispersed accretionary and scoriaceous lapilli layers. At Section 9B (Fig. 3F) the upper phreatomagmatic unit, clearly overthickened at the base of a steeply inclined hillslope, infills an eroded lower scoriaceous fall unit suggesting a brief hiatus between these two syn-eruptive events. At all other sections in this sector both units appear conformable without any indication of an intervening break or soil development. At Section 9D (Fig. 3E) the basal scoriaceous lapilli bed is itself underlain by a centimeter (cm)-thick surge deposit comprising compact, brownish gray, low-angle cross-bedded fine to medium ash with few medium-scoriaceous lapilli dispersed randomly throughout. This surge deposit appears localized and probably relates to its passage down an isolated stream tributary.

Further north, at Section 4 on the southern side of a formerly glaciated mountain pass (~264 m a.s.l) separating Lago Blanco (south) with Lago Negro (north) the stratigraphy of Lepué Tephra is well exposed (Fig. 4). Here, the stratigraphy reveals a prominent (meter-thick) rhyolitic pumiceous lapilli fall unit (Cha-1 *senso stricto* Naranjo and Stern, 2004; dated at *c.* 8700 ^{14}C a BP, Watt *et al.*, 2011) sourced from an

Copyright © 2017 John Wiley & Sons, Ltd.

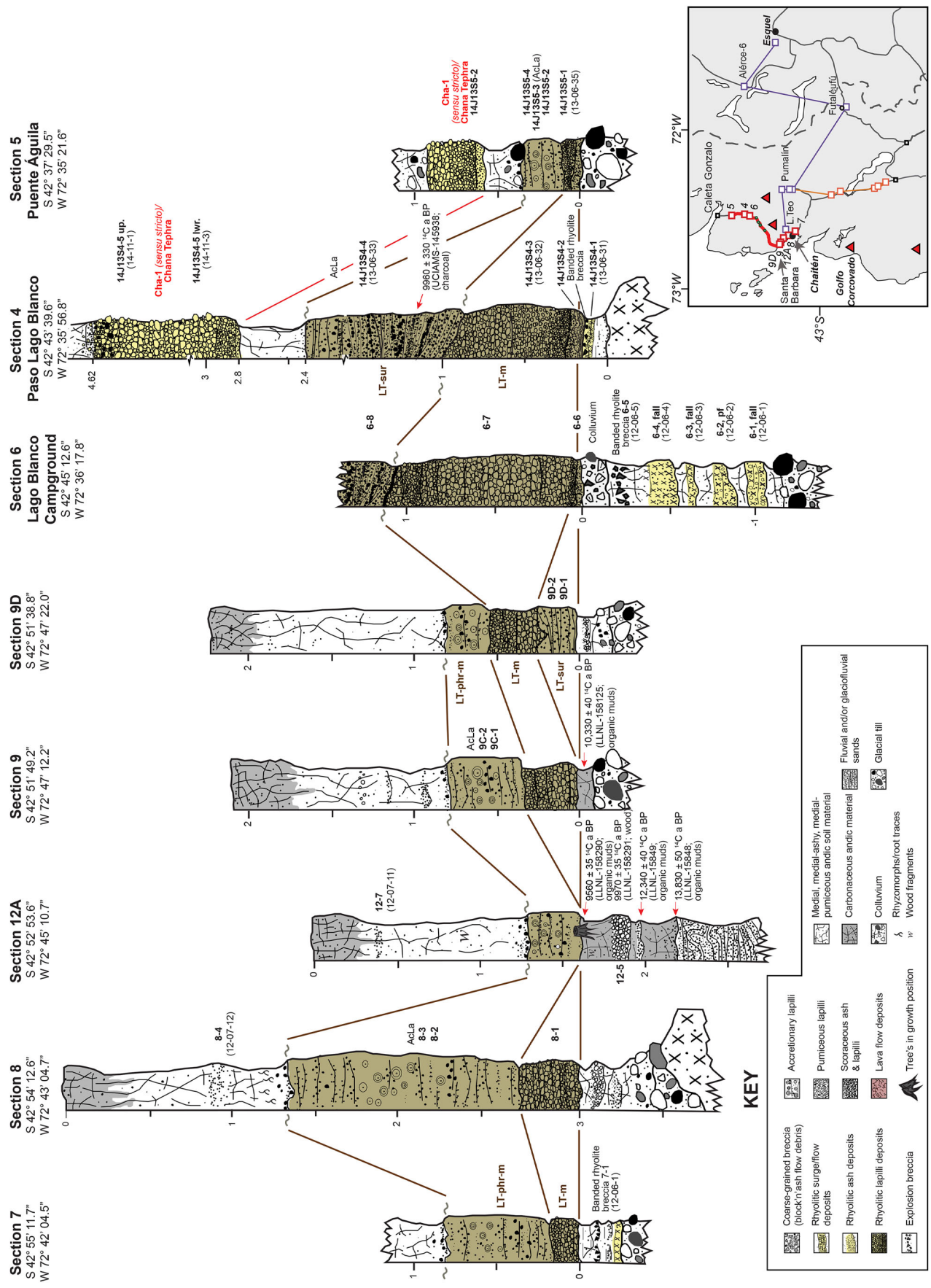

Figure 2. Stratigraphic columns showing the correlation of Lepué Tephra and enveloping tephra beds from Section 7 located within Chaitén township northward to Section 5 at Puente Águila on Ruta 7, 8.2 km south of Caleta Gonzalo.

Copyright © 2017 John Wiley & Sons, Ltd.

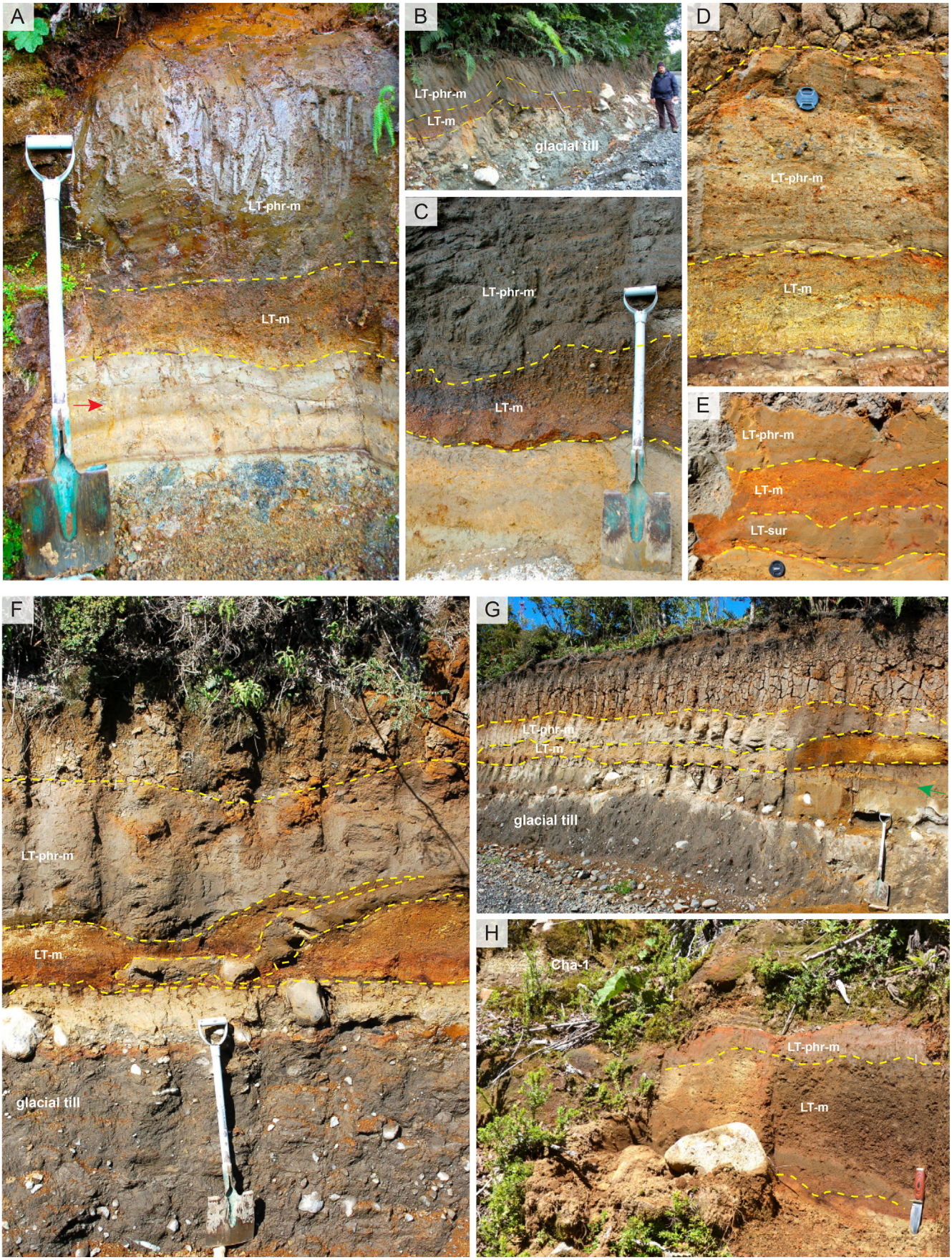

Figure 3. Lepué Tephra at Sections 7 (A), 8 (B, C), 9 (D), 9D (E), 9B (F, G) and 5 (H) that illustrate the complex internal architecture of magmatic (LT-m) and phreatomagmatic (LT-phr-m) fall and flow (LT-sur) co-eruptive phases (Fig. 2). Arrows in A and G indicate the position of highly weathered cm-thick ash and lapilli beds of unknown eruptive origin.

Copyright © 2017 John Wiley & Sons, Ltd.

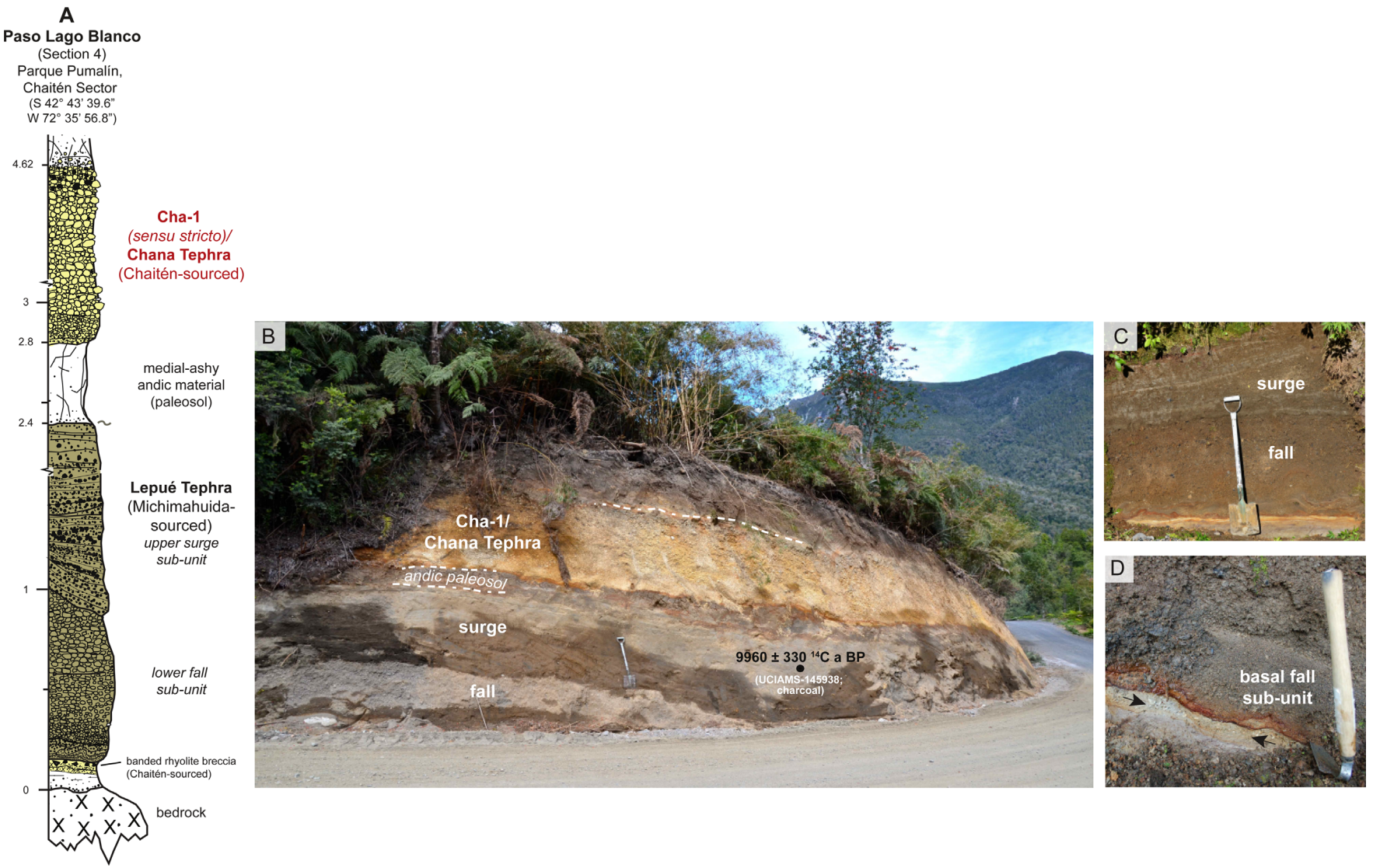

Figure 4. (A) The stratigraphy of Section 4 located on Ruta 7 on the southern side of the pass connecting Lago Blanco (south) with Lago Negro (north). The stratigraphy at this section reveals a prominent rhyolitic pumiceous lapilli (Cha-1 *sensu stricto*) dated at *c.* 8700 ^{14}C a BP and sourced from an ancestral Chaitén Volcano. (B) Cha-1 tephra (now formally renamed Chana Tephra; Alloway *et al.*, 2017) closely overlies a lower fall and surge co-eruptive couplet (Lepué Tephra) of presumed Michimahuida source. The surge deposit is directly dated at 11 483 ± 1034 cal a BP (9960 ± 330 ^{14}C a BP; UCIAMS-145938). The spade is 1 m in length. (C) Low-angle cross-bedding and cross-cutting relationship of the surge across its co-eruptive fall deposit. (D) The entire sequence is underlain by a widespread and distinctive layer of banded rhyolite breccia (indicated by arrows) that probably represents an explosion of a pre-Cha-1/Chana Tephra lava dome (ancestral VCha).

Copyright © 2017 John Wiley & Sons, Ltd.

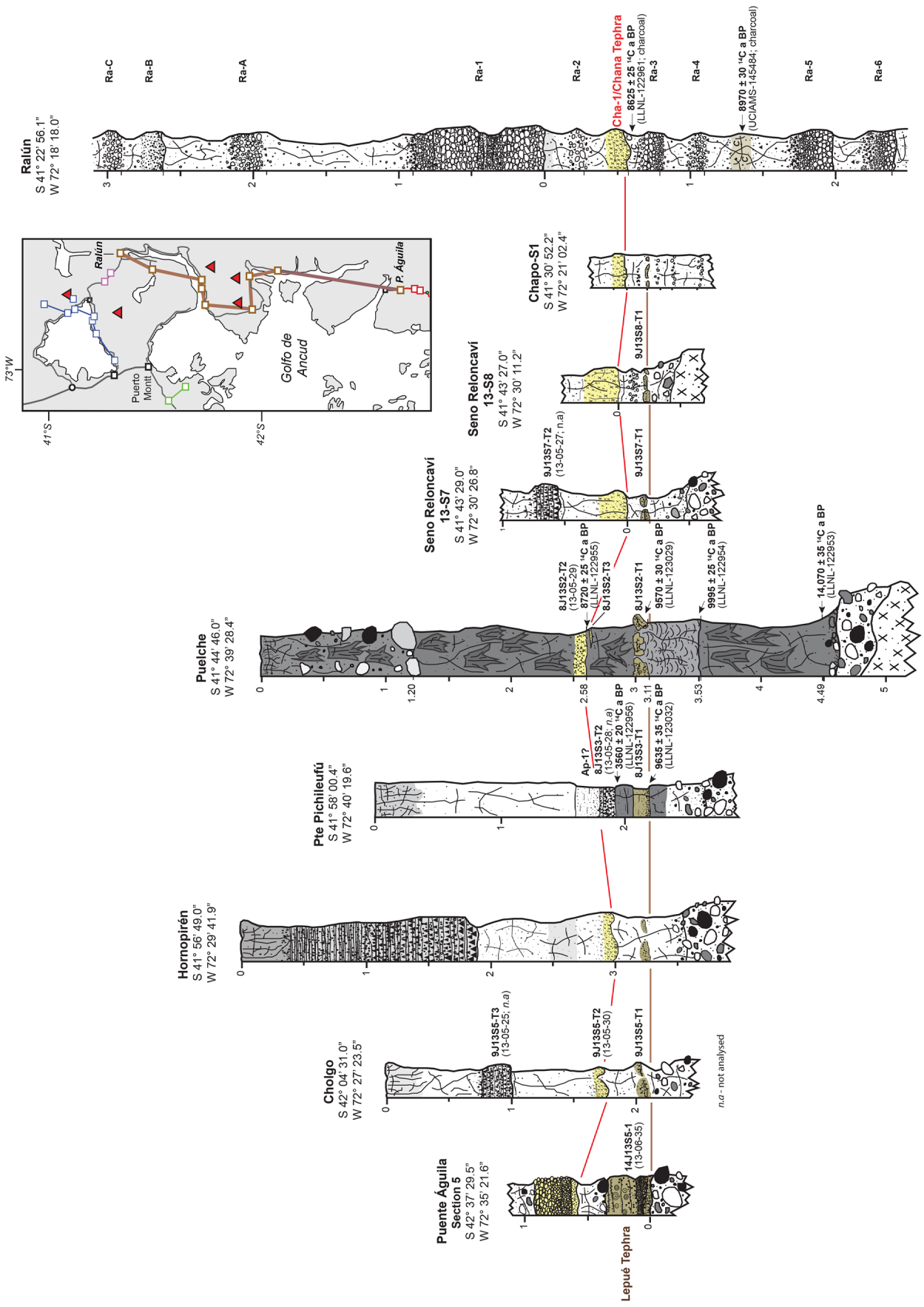

Figure 5. Stratigraphic columns showing the correlation of Lepué Tephra and enveloping tephra beds from Section 5 at Puente Águila northwards to sections located near Seno Reloncaví and Ralún. Note the closely overlying occurrence of Cha-1 (now formally named Chana Tephra, see Alloway *et al.*, 2017) sourced from VCha.

Copyright © 2017 John Wiley & Sons, Ltd.

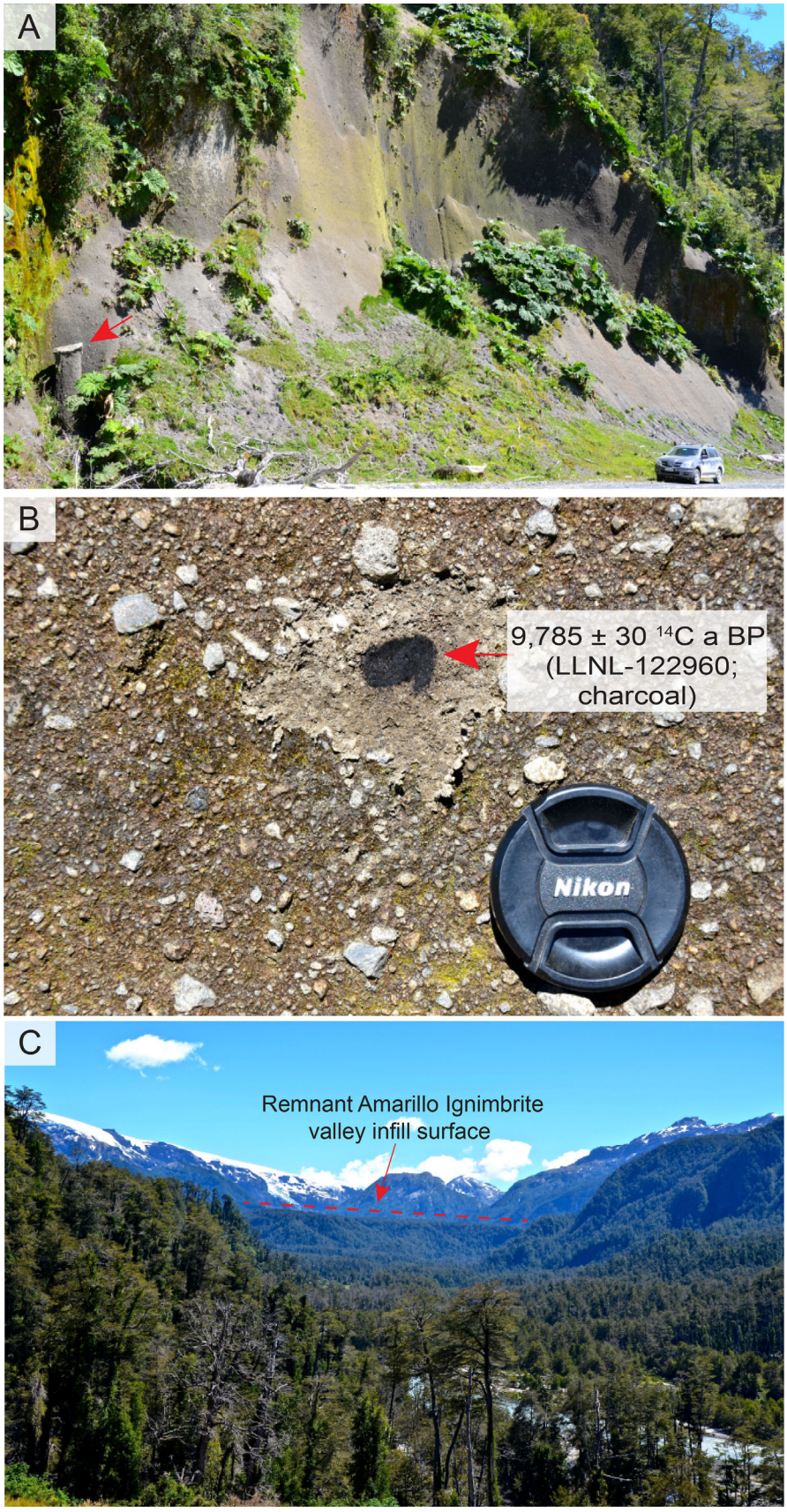

Figure 6. (A) Massive > 40-m-thick pyroclastic density current (PDC) deposit exposed at Pumalín-1 (Pum-1) section along road W-887 located directly adjacent to Río Michimahuida. This PDC deposit correlates with Amarillo Ignimbrite of Amigo *et al.* (2013) and is considered contemporaneous with Lepué Tephra on the basis of its equivalent stratigraphic position and age. Arrow indicates orientated, meter-sized, lithic clast transported within this PDC. (B) Typical PDC internal architecture with dispersed poorly sorted, angular, lithic clasts and rare charcoal fragments that are dated at 11 190 ± 88 cal a BP (9785 ± 30 ^{14}C a BP; LLNL-122960). (C) Remnant Amarillo Ignimbrite valley-infill surface viewed north-west from W-887 roadside lookout (42°55′18.33″S, 72°23′46.99″W; ~436 m asl). Note that this surface is clearly inclined towards the Michimahuida massif (tMim).

ancestral VCha, separated from a lower scoriaceous surge and fall couplet below by ~0.4 m of medial-ashy andic material (paleosol). This lower couplet is characterized by a basal fall subunit characterized by multiple, normal graded cm-thick beds of well-sorted coarse to very-fine sand-textured scoriaceous ash, grading upwards to a more prominent fall subunit comprising weakly stratified, poorly sorted, scoriaceous coarse lapilli. This fall unit is unconformably overlain by a surge unit containing conspicuous, moderately sorted, inclined planar to low-angle cross-bedded, scoriaceous ash and lapilli beds. Charcoal fragments retrieved from within this upper surge unit were dated at 11 483 ± 1034 cal a BP

Copyright © 2017 John Wiley & Sons, Ltd.

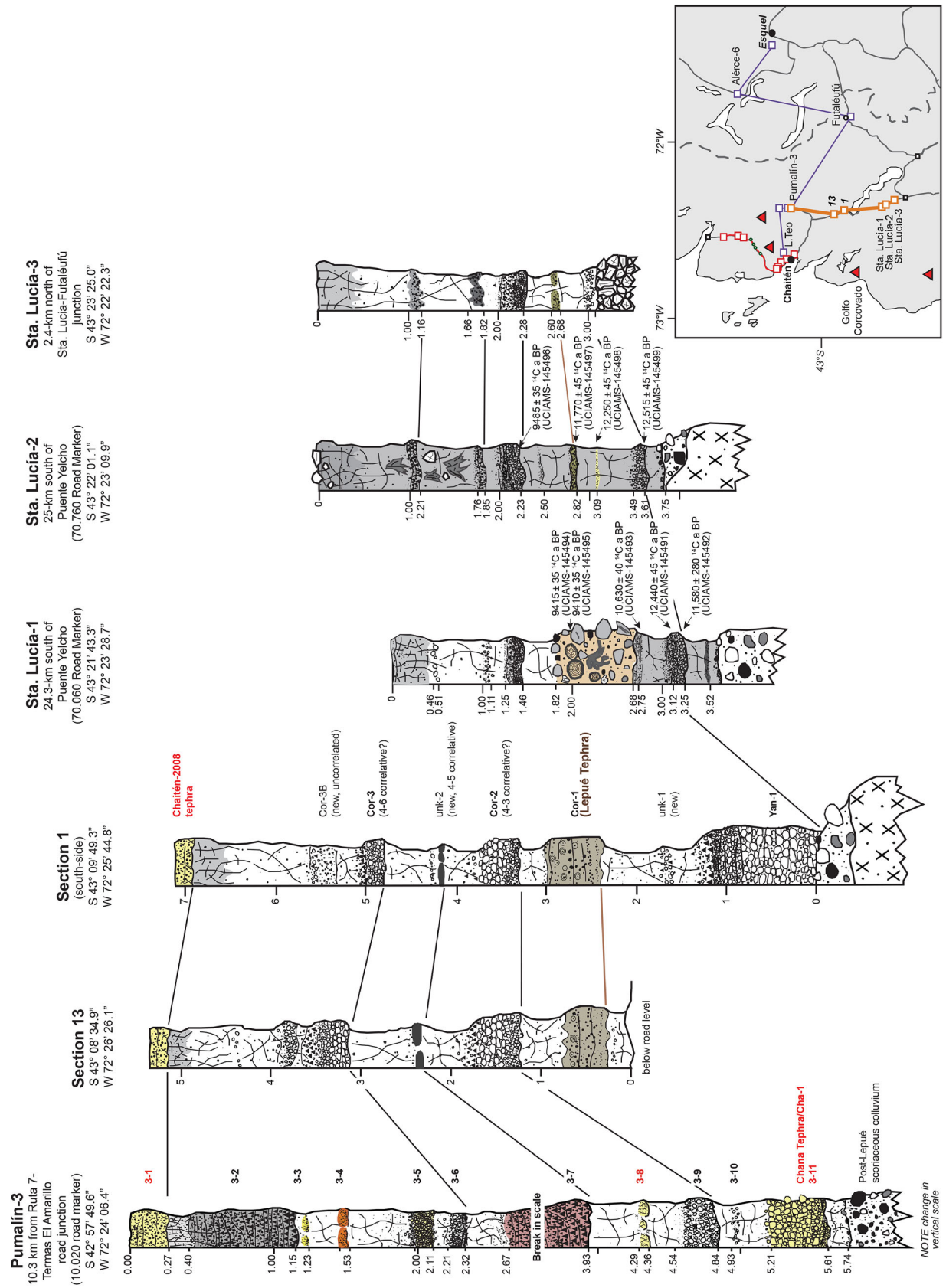

Figure 7. Stratigraphic columns showing the correlation of Lepué Tephra and enveloping tephra beds from Section Pumalín-3 southward to Santa Lucía-3, ~ 2.4 km north of the Sta. Lucía–Futaleufú junction. Note the occurrence of a diamict (1.82–2.68 m below surface) within Sta. Lucía-1 containing fragmental rock clasts, wood and organic rip-up clasts (dated at c. 9400 ^{14}C a BP; c. 10 600 cal a BP). The internal architecture strongly suggests deposition from a debris avalanche event. Although the erosional base of this debris avalanche deposit is associated with a prominent tephra, the two events do not appear to be chronologically related. On this basis it seems more likely that this catastrophic avalanche event was probably triggered by tectonic seismicity.

Copyright © 2017 John Wiley & Sons, Ltd.

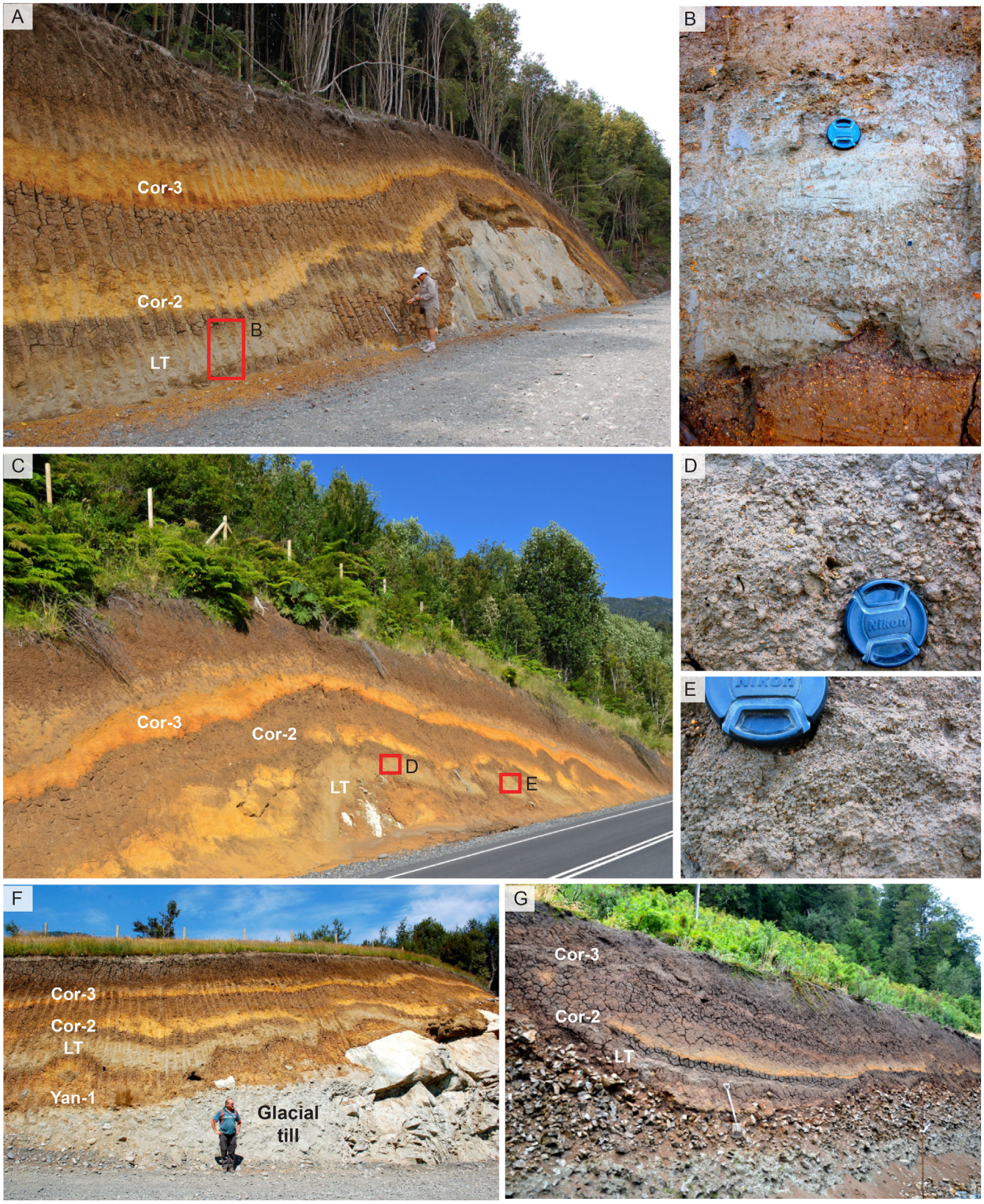

Figure 8. Lepué Tephra at Sections 1 (A), 13 (B) and 14 (C, D, E) of the southern transect (Fig. 7). Here, Lepué Tephra is dominated by compact gray, poorly sorted and crudely stratified 'lapilli-tuff' deposits (phreatomagmatic phase) containing dispersed cm-sized accretionary lapilli (D) and obvious open interstitial pore spaces (E) indicative of rain flushing. No co-eruptive magmatic phase was identified.

(9960 ± 330 ^{14}C a BP; UCIAMS-145938) and are distinguishable from those radiocarbon ages acquired for Lepué Tephra correlatives elsewhere (see Age Section). At Section 4, Lepué Tephra (represented as a fall–flow couplet) is closely underlain by widespread and distinctive layers of banded rhyolite breccia and rhyolitic ashy material unconformably overlying basement bedrock. This layer of rhyolitic breccia underlying Lepué Tephra can be correlated to Section 6 (Lago Blanco) and Section 7 (within Chaitén township) (Fig. 2) and probably represents explosive fragmental debris originating from a

Copyright © 2017 John Wiley & Sons, Ltd.

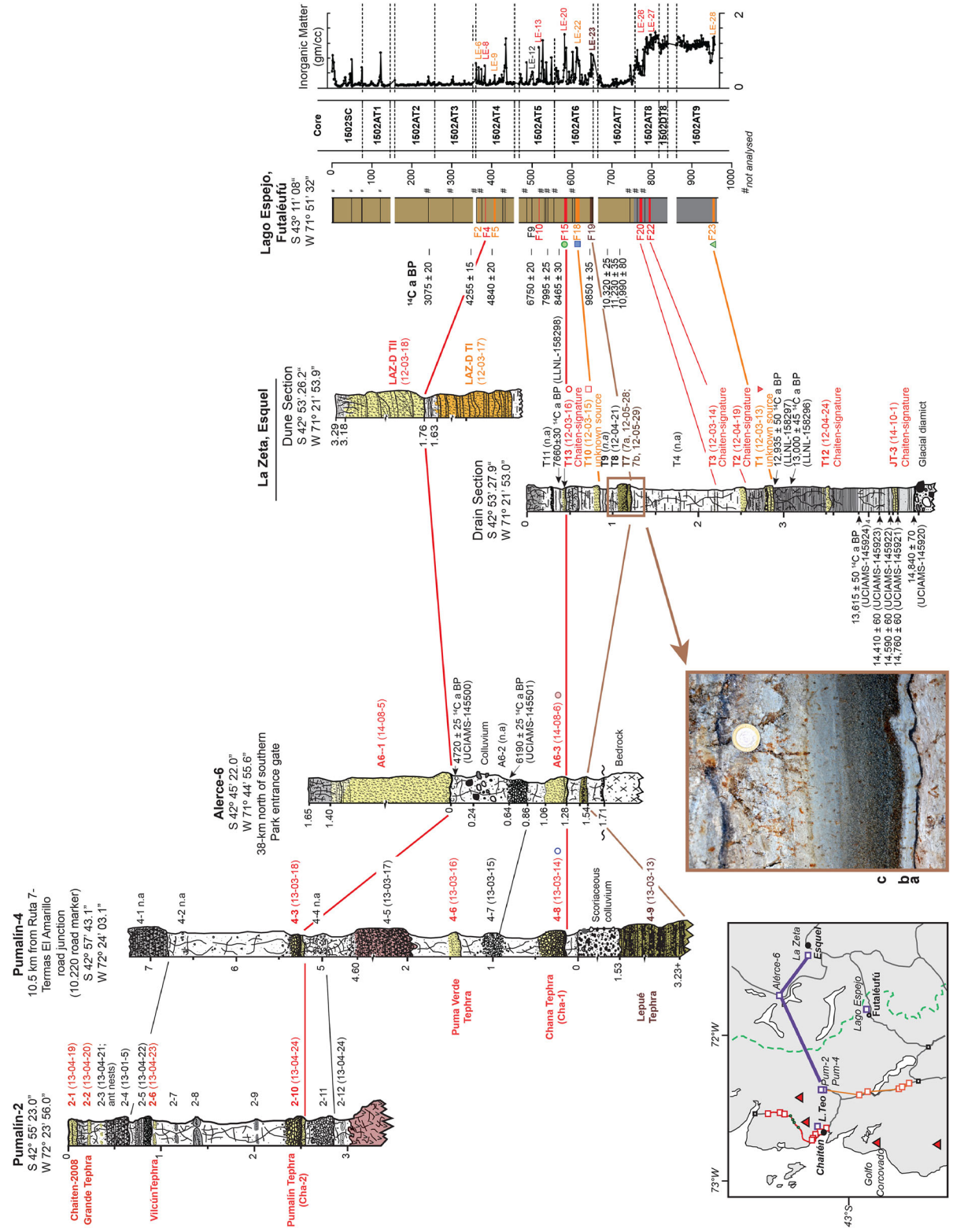

Figure 9. Stratigraphic columns showing the correlation of Lepué Tephra and enveloping tephra beds from Section Pumalín-2 eastwards to La Zeta 3 km west of Esquel in Argentina. A lake record from Lago Espejo, Futaleufú, Chile, is also included to show correlation of Lepué Tephra as well as rhyolitic tephra sourced from an ancestral Volcan Chaitén. The inset photo shows Lepué Tephra as preserved enveloped by paleolake sediments at La Zeta. Note the well-defined shower bedding with a thin, well-sorted coarse ash base (initial magmatic phase) overlain by compact, gray, poorly sorted massive structured very fine ash (phreatomagmatic phase) followed by proportionally thicker normal-graded moderately well-sorted very coarse to fine ash (magmatic phase). This eruptive architecture is in accord with features from more proximal localities that similarly indicate a complex phreatomagmatic-magmatic eruption style for Lepué Tephra.

Copyright © 2017 John Wiley & Sons, Ltd.

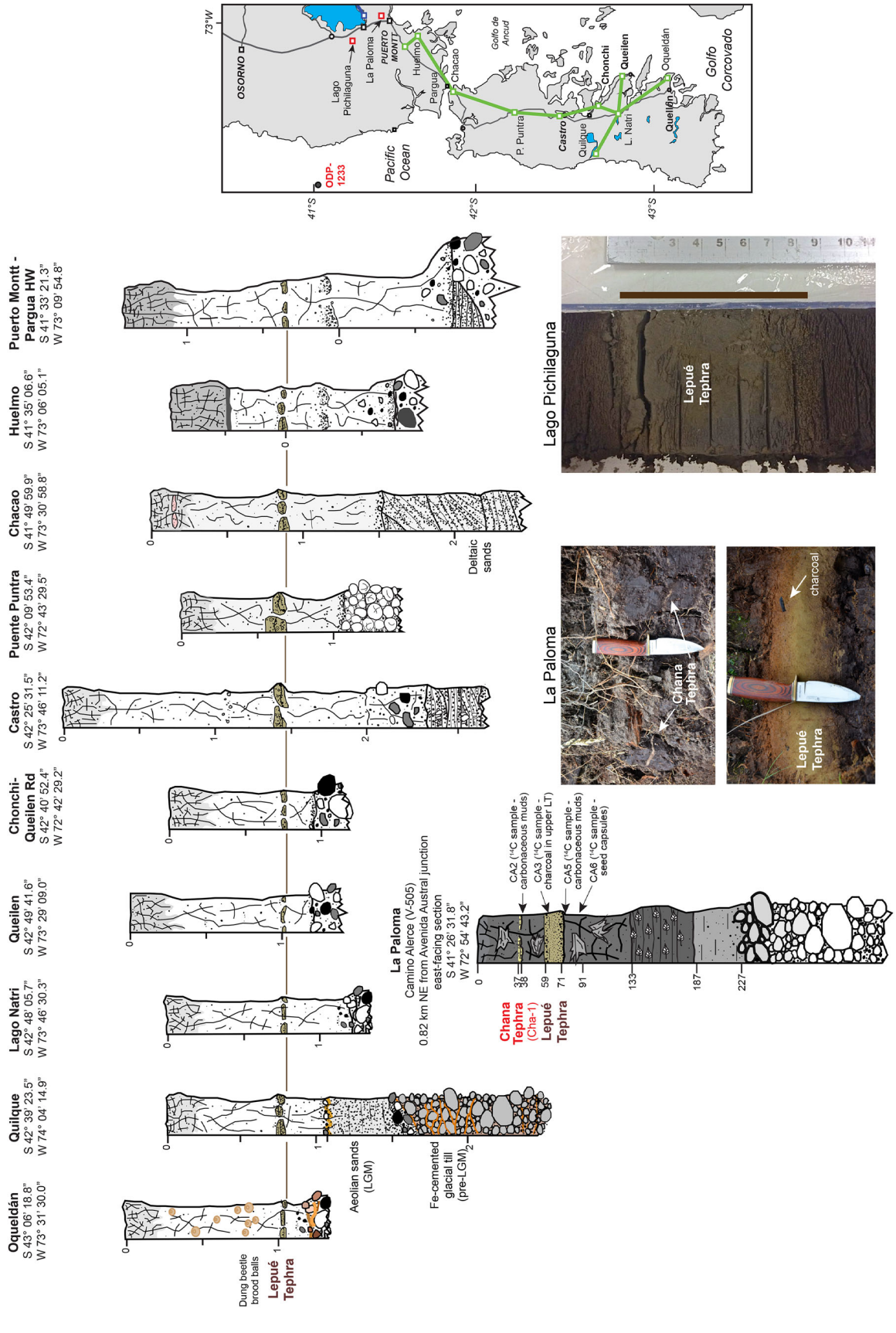

Figure 10. Stratigraphic columns showing the correlation of Lepué Tephra along the western transect from south-central Isla Grande de Chiloé northward towards Puerto Montt in southernmost continental Chile. In northern sections (i.e. Huelmo and along Ruta 5 connecting Pargua with Puerto Montt) Lepué Tephra is closely underlain by intensely weathered andesitic ash and lapilli 'ghosts' that are probably derived from either Volcanes Calbuco or Yate located to the east along the Andean mountain divide. These weathered tephra have yet to be geochemically characterized. At the La Paloma site located between Puerto Montt and Alerce, Lepué Tephra forms a continuous layer ~12 cm thick within peat and is closely overlain (~20 cm) by a discontinuous and irregularly thick (<1 cm) layer of Cha-1 (Chana Tephra). The other photo inset shows the Lepué Tephra at its northernmost occurrence within Lago Pichilaguna, immediately west of Llanquihue township and 180 km north-west of Volcán Michimahuida. Here, Lepué Tephra occurs within core 1402AT3 at 382–390 cm depth as a ~8-cm-thick dark olive-gray, normally graded coarse to very fine ash. In this same vicinity, Lepué Tephra is not recognized macroscopically within the andic soil-forming environment.

Copyright © 2017 John Wiley & Sons, Ltd.

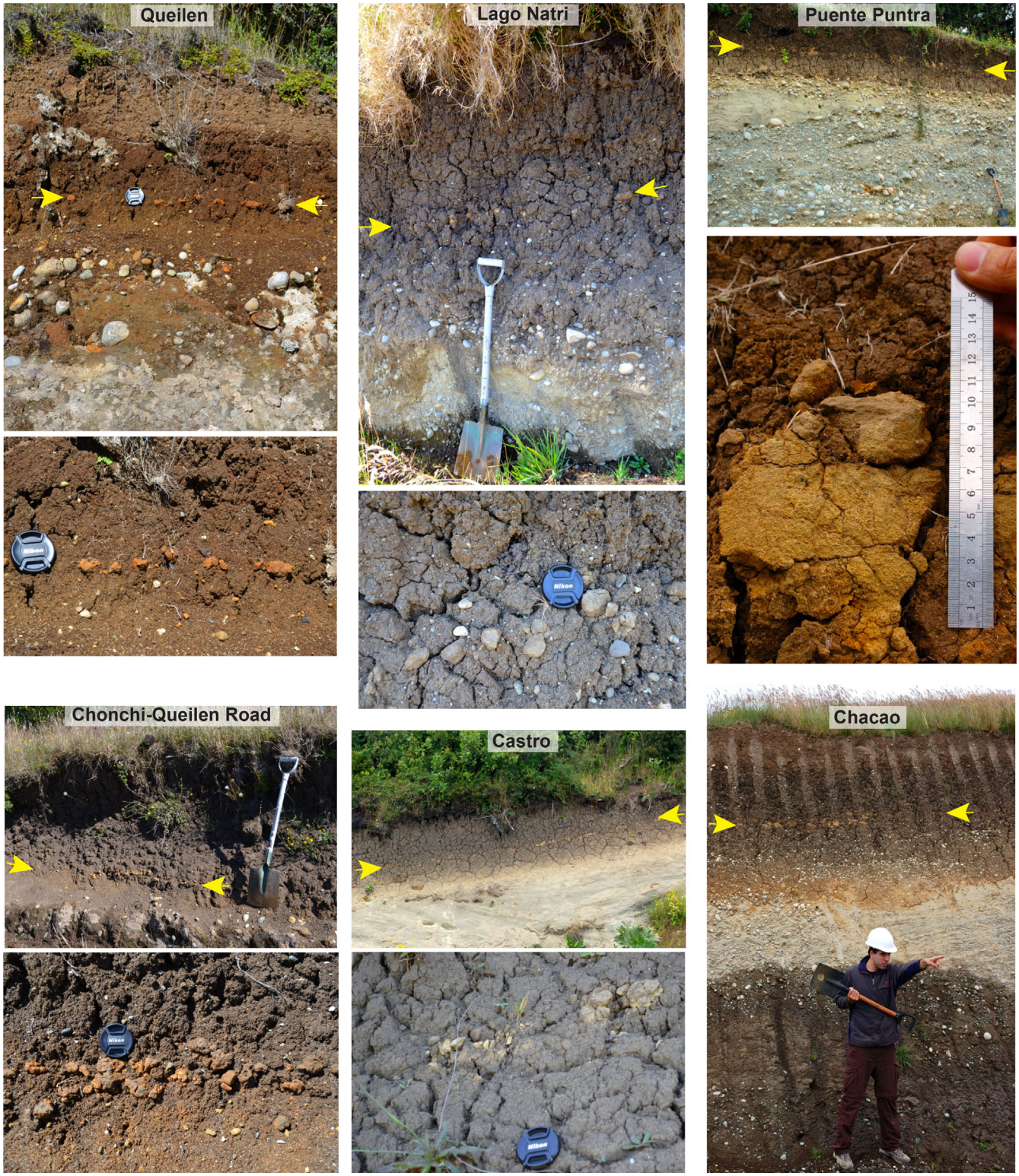

Figure 11. The variable morphological expression of Lepué Tephra within cover-bed sections (Queilen, Lago Natri, Chonchi, Castro, Puente Puntra and Chacao) in Isla Grande de Chiloé (Fig. 10). The position of Lepué Tephra is indicated by yellow arrows. At all sections in this sector Lepué Tephra is the only macroscopic tephra observable within the cover-bed sequence and forms highly irregular, discontinuous pods of cemented fine ash. Typically in this sector, Lepué Tephra is enveloped by andic soil material and closely overlies colluvium, bedded fluvio-glacial gravels and sands and glacial diamictons (till). In cases where Lepué Tephra closely overlies impermeable glacial diamictons which seasonally perch the local water table, tephra colour is strongly altered to strong brown chromas, whereas Lepué Tephra enveloped by thicker successions of free-draining andic soil material typically has gray to pale brown chromas.

pre-Cha-1 lava dome (ancestral VCha). Such pre-Cha-1 rhyolitic sequences are rarely observed proximal to an inferred source due to deep burial and/or pervasive Andean glaciation (Alloway *et al.*, 2017).

Northwards along the continental coastline (Fig. 5), Lepué Tephra can be reliably traced from Section 5 at Puente Águila to sections near Seno Reloncaví. In most sections, Lepué Tephra is subtly expressed within the andic soil material as laterally discontinuous cemented aggregates of olive-brown to reddish-brown fine to medium ash. Often Lepué Tephra is stratigraphically associated with Cha-1 tephra above (Fig. 5). At Puente Pichileufú on the Hualaihue Peninsula, Lepué

Copyright © 2017 John Wiley & Sons, Ltd.

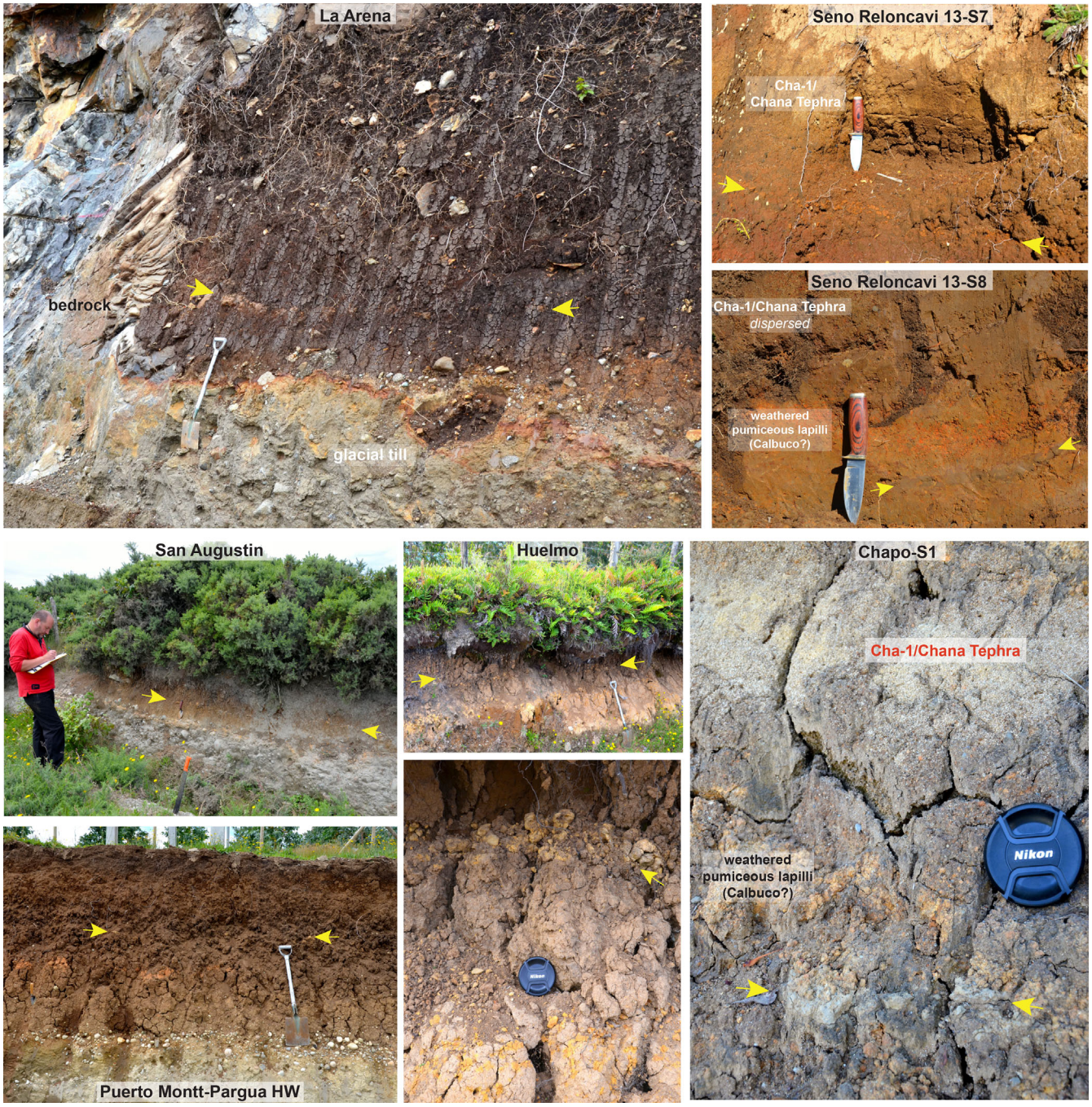

Figure 12. Lepué Tephra (indicated between yellow arrows) occurring within cover-bed sections in southernmost continental Chile (San Augustin, Huelmo and Ruta 5 connecting Pargua with Puerto Montt). Sections (Caleta La Arena, 13-S7, 13-S8, Chapo S1) near Seno Reloncaví are also shown (Figs 5 and 10). Note that Cha-1 is now formally renamed Chana Tephra (Alloway *et al.*, 2017).

Tephra is unconformably overlain by a scoriaceous coarse ash bed of presumed Apagado-source (Ap-1? of Watt *et al.*, 2011), whereas further north-eastwards (i.e. Chapo-S1) towards Ralún, Lepué Tephra is enveloped by a steadily increasing number of discontinuous weathered lapilli of presumed Calbuco-source dispersed in andic medial material.

Relationship with pyroclastic flow and surge deposits

In sections along road W-887 located directly adjacent to Río Michimahuida (i.e. Pumalín Section 1), a massive > 40-m-thick unconsolidated lithic-rich pyroclastic density current (PDC) deposit can be observed with meter-sized oriented lithic intraclasts and rare, dispersed cm-sized charred wood fragments (Fig. 6A,B). At other sections along road W-887 (i.e. Pumalín-4), syneruptive fall deposits that overlie this PDC deposit can occasionally be observed. At these sections, the uppermost co-eruptive scoriaceous fall deposits are separated from Cha-1 above (i.e. Pum 4-T8) by a pervasive wedge of colluvial debris of mixed lithologies indicating widespread landscape instability in the devastating aftermath of this eruption. Northward from the W-887 road-end, an extensive elevated sloping remnant valley-fill surface can be clearly observed within the confines of the glacially dissected Río Michimahuida valley and extending down to the Río Mallines–Michimahuida confluence (Fig. 6C). This same PDC deposit and surface was recognized by Amigo *et al.* (2013) and named Amarillo Ignimbrite. Two radiocarbon samples

Copyright © 2017 John Wiley & Sons, Ltd.

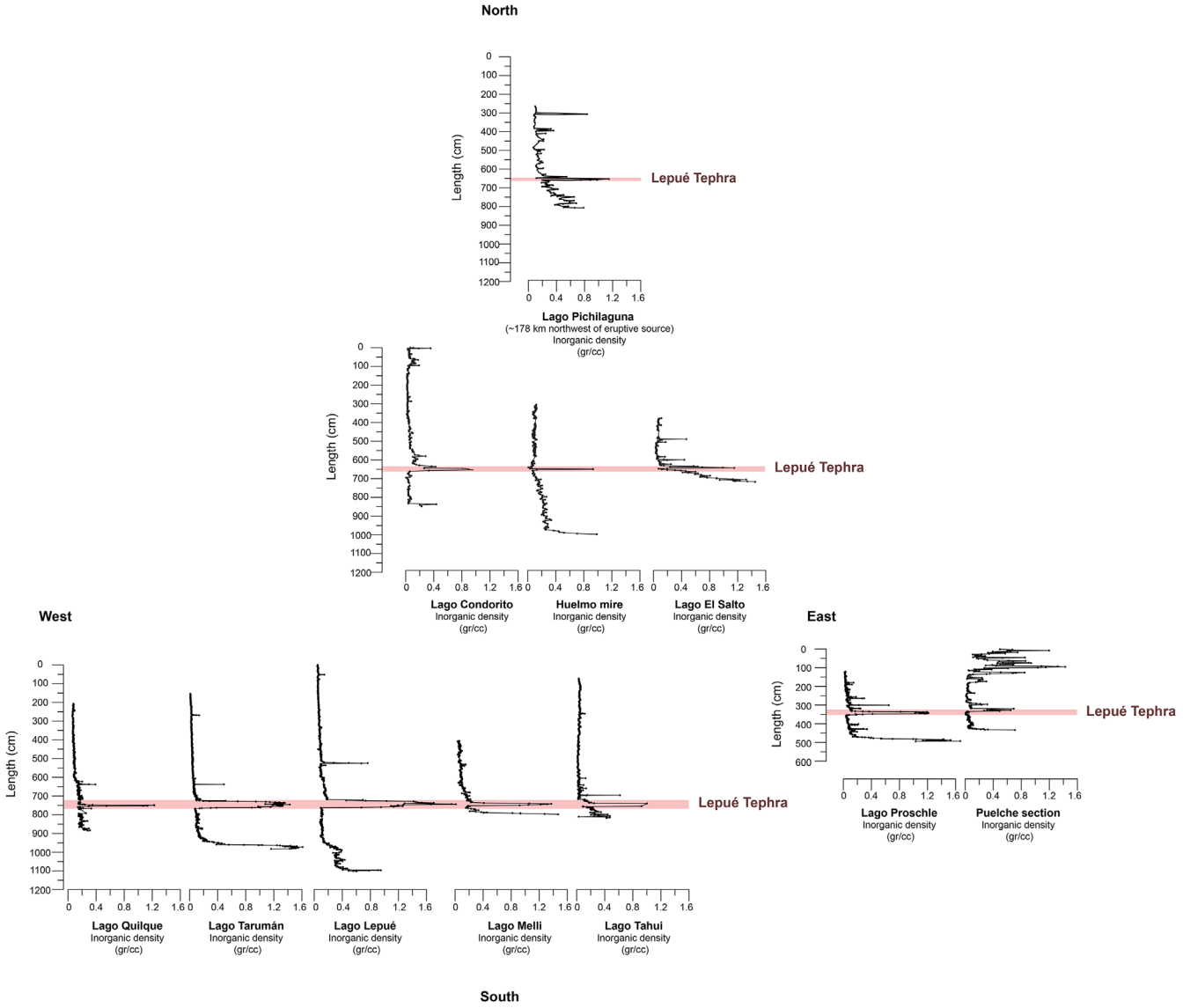

Figure 13. Down-core inorganic densities ($g\,ml^{-1}$) of lake sediments retrieved from Isla Grande de Chiloé (i.e. Quilque, Tarumán, Lepué, Melli and Tahui), coastal continental lakes and mires east of Golfo de Ancud (Lago Proschle and Puelche), south (i.e. Condorito, Huelmo, El Salto) and north (i.e. Pichilaguna) of Puerto Montt. The occurrence of Lepué Tephra is strongly indicated in all records and is closely overlain by a subordinate peak. This lesser peak (i.e. Isla Grande de Chiloé sites) probably coincides with a *c.* 8 cal ka Chaitén-sourced rhyolitic cryptotephra (Puma Verde Tephra, see Alloway *et al.*, 2017), which unlike Lepué Tephra is not typically expressed macroscopically in adjacent andic soil cover-beds.

acquired from within and just above the Amarillo Ignimbrite were dated at 9260 ± 50 and 9510 ± 50 ^{14}C a BP, respectively, and are broadly in accord with an age of 9785 ± 30 ^{14}C a BP (LLNL-122960) from our sample retrieved from Pumalín-1. These ages are also indistinguishable from a radiocarbon age associated with the prominent surge deposit occurring at Section 4 in the north-western sector of Michimahuida (Fig. 4). While the voluminous scoriaceous-rich PDC deposit can be clearly identified in both the south-eastern and the north-western sectors of tMim, the precise location of the eruptive source vent is obscured by ice fields and is currently unknown.

Southern sectors

At Sections 1, 13 and 14 located on Ruta 7 between Amarillo and Puerto Cárdenas (Figs 7 and 8), Lepué Tephra (previously referred to as *Cor-1* by Naranjo and Stern, 2004) is enveloped by a sequence of at least six cm- to dm-thick, basaltic-andesite to andesitic ash and lapilli inter-beds within dominantly reddish brown andic soil material that typically overlies glacial diamict (till) draping bedrock. While some of these enveloping tephra (i.e. Unk-2) can be reliably traced northwards towards Michimahuida, the eruptive origins of the majority (i.e. Yan-1, Cor-2 and Cor-3 named by Naranjo and Stern, 2004) have yet to be determined. In this sector, Lepué Tephra is typically characterized by a dm-thick weakly stratified, brownish gray, very poorly sorted cemented ash with indistinct cm-sized accretionary lapilli and scoriaceous lapilli-rich ashy intrabeds. Cemented fine ash frequently contains open interstitial pore spaces, which are typically indicative of syn-depositional rain flushing (Fig. 8). Beneath this cemented gray ash are common, highly weathered reddish-brown scoriaceous fine to very fine lapilli dispersed within underlying medial andic material. Lepué Tephra can be traced south to near Santa Lucía where it occurs as a laterally discontinuous, variably thick (8–13 cm) gray cemented fine ash intervening between Yan-1 and Cor-2 correlatives above clast-supported breccia (talus deposit).

Eastern sectors

Lepué Tephra can be reliably correlated eastwards to distal sections in Chile (Lago Espejo, Futaleufú) and Argentina

Copyright © 2017 John Wiley & Sons, Ltd.

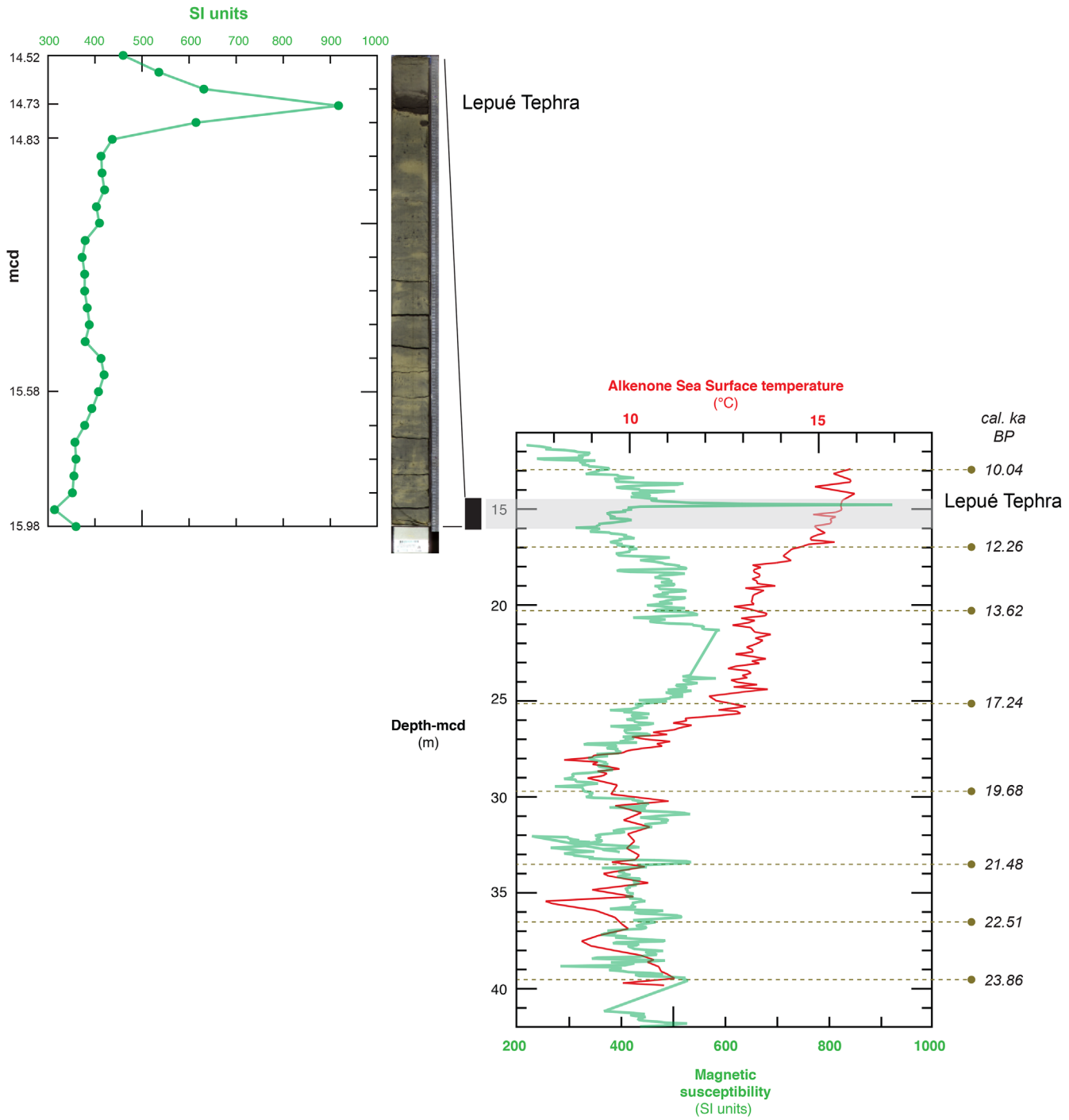

Figure 14. Magnetic susceptibility (SI units; indicated in green) and alkenone-based sea surface temperature estimates (°C) of ODP-202 Site-1233 (indicated in red). The positions of calibrated radiocarbon ages are indicated on the right. The inset shows a prominent macroscopic tephra encapsulated within clay and silty clays between 14.52 and 14.83 mcd and is accompanied by a prominent spike in magnetic susceptibility (916.8-m mol^{-1} (SI)). Unfortunately, no radiocarbon dates were obtained directly associated with the upper and lower contacts of this tephra but bracketing radiocarbon samples from 12.94 and 17.01 mcd yielded calibrated ages of 10 040 and 12 260 cal a BP, respectively.

(Alerce-6 and La Zeta) (Fig. 9). Correlation is based on a combination of morphological expression, chronostratigraphic association and correspondence of glass shard major element compositions. The Lepué Tephra correlative at Lago Espejo, Alerce-6 and La Zeta is overlain by two prominent rhyolitic coarse ash beds that can be correlated with Cha-2 and Cha-1 tephras dated at *c.* 4950 and 9750 cal a BP, respectively (Watt *et al.*, 2013). At La Zeta, an ~11-cm-thick tephra is prominently expressed within an ~ 5-m-thick lake sequence that contains numerous other mm- to cm-thick tephra inter-beds of basaltic through to rhyolitic compositions. A radiocarbon age (14 840 ± 70 ^{14}C a BP; UCIAMS-145920) from basal lake sediments directly overlying glacial diamict (till) establishes a maximum age of ~17 800 cal a BP for the lake sequence. While the Lepué Tephra correlative at La Zeta is not directly dated, it is loosely constrained by radiocarbon dates obtained from enveloping tephra inter-beds within the lake sequence. Certainty of correlation is achieved by glass shard major element chemistry (see below).

At La Zeta, the Lepué Tephra correlative consists of three distinct fall units. The lowermost unit consists of dark gray well-sorted coarse ash (<1 cm thick, layer 'a' in Fig. 9 photo inset). This unit is overlain by a compact, subtly bedded, pale gray, moderately sorted fine to very fine ash (~2 cm thick, layer 'b' in

Copyright © 2017 John Wiley & Sons, Ltd.

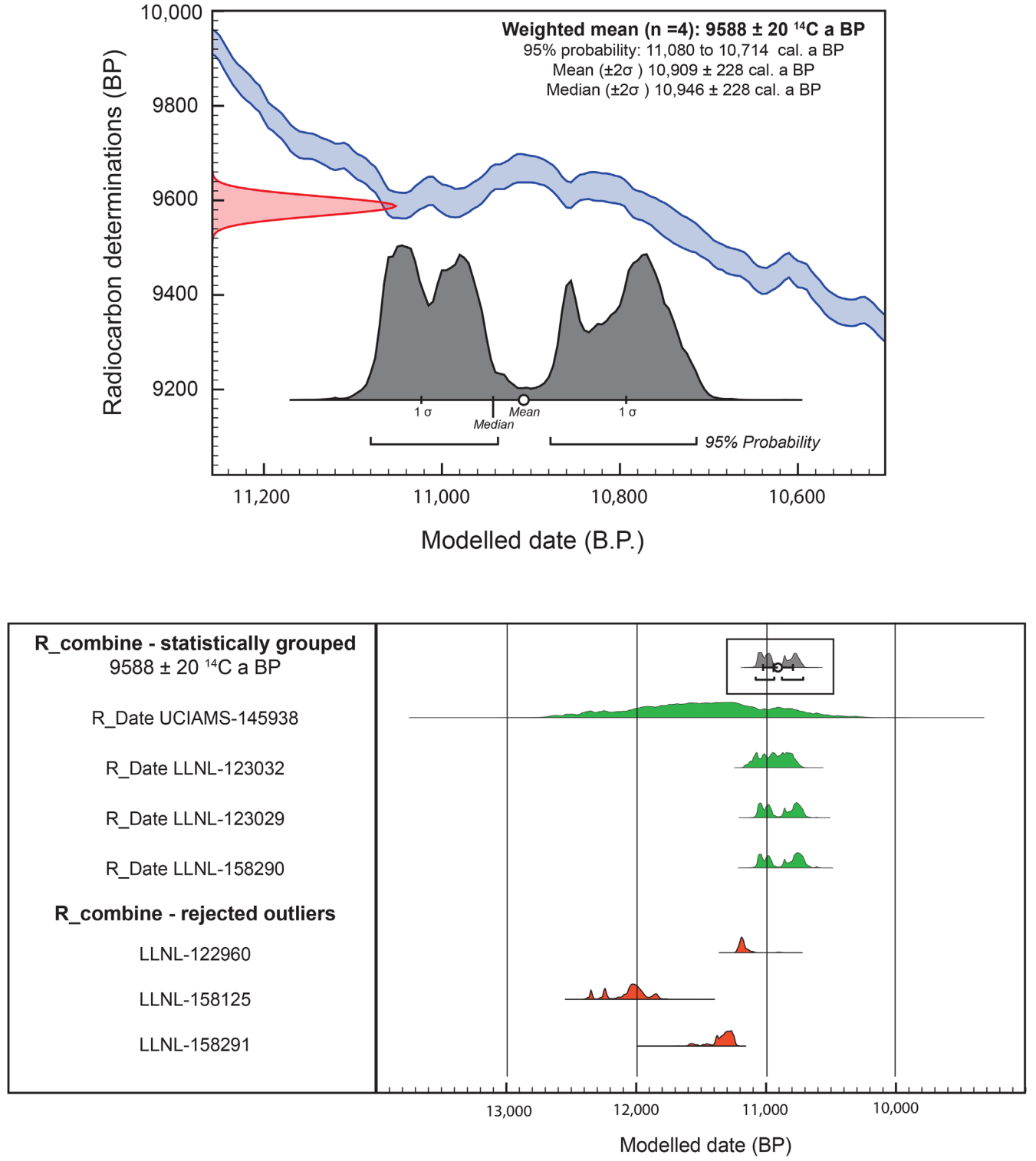

Figure 15. Weighted mean modeled age determination (9588 ± 20 ^{14}C a BP) for Lepué Tephra based on four R-combine-statistically grouped samples (UCIAMS-145938, LLNL-158290, LLNL-123032 and LLNL-12329) from Sections 4 and 12A, Pichileufú and Puelche, respectively. Three ^{14}C sample outliers from Sections 9 and 12A and Pumalín-1, (LLNL-158125, LLNL-158291 and LLNL-122960) were rejected. The Southern Hemisphere terrestrial calibration curve (SHCal13) and OxCal Program (v.4.2.4) were used for all samples radiocarbon dated in this study.

photo inset) which in turn is overlain by an ~8-cm-thick uppermost unit (layer 'c' in photo inset) comprising loose, well-sorted, very coarse to fine, gray scoriaceous ash. The internal architecture of Lepué Tephra at this locality affirms the complex phreatomagmatic to magmatic origin of this deposit.

Western sectors

Through most of Isla Grande de Chiloé and its adjacent islands, Lepué Tephra is the only macroscopic tephra that can be systematically observed within the late last glacial to post-glacial andic cover-beds. Stratigraphic columns show the correlation of Lepué Tephra along a western transect from south-central Isla Grande de Chiloé northwards towards Puerto Montt in southernmost continental Chile (Fig. 10). Typically in this sector, Lepué Tephra forms highly irregular, discontinuous pods of crudely bedded, cemented fine- to medium-ash enveloped by reddish brown andic soil material and closely overlying late last glacial to LGM colluvium, bedded fluvio-glacial gravels and sands,

Copyright © 2017 John Wiley & Sons, Ltd.

Table 1. Radiocarbon dates and ages associated with Lepué Tephra and its distal correlatives. The Southern Hemisphere terrestrial calibration curve (SHCal13) and OxCal Program (v.4.2.4) were used for all radiocarbon samples dated in this study.

Location	Lab. ID	Sample type	Sample position	14C AMS age (14C a BP)	Calibrated* age (±2σ) (cal a BP)	95% HPDF† (cal a BP)
Onshore *(this study)*						
S-4, Chaitén†	UCIAMS-145938	Charcoal (twig)	Within-surge deposit (co-eruptive correlative)	9960 ± 330	11 483 ± 1034	10 561–12 552
Pumalín-1, Chaitén	LLNL-122960	Charcoal (outer small tree)	Within pyroclastic deposit (co-eruptive correlative)	9785 ± 30	11 190 ± 88	11 108–11 237
Pte Pichileufú†	LLNL-123032	Bulk carbonac. muds	Immediately below lower contact	9635 ± 35	10 934 ± 118	10 753–11 134
Puelche†	LLNL-123029	Bulk highly carbonac. muds	Immediately below lower contact	9570 ± 30	10 862 ± 250	10 595–11 080
S-9, Chaitén	LLNL-158125	Bulk carbonac. muds	Immediately below lower contact	10 330 ± 40	12 033 ± 280	11 825–12 383
S-12A, Chaitén†	LLNL-158290	Bulk carbonac. muds	Immediately below lower contact	9560 ± 35	10.841 ± 262	10 563–11 081
	LLNL-158291	Wood in growth position	Immediately below lower contact	9970 ± 35	11 321 ± 170	11 234–11 500
R_combine modeled age (n = 4†)				**9588 ± 20**	**10 909 ± 228**	**10 714–11 080**
(Previous studies)						
Huelmo (Moreno and Leon, 2003)	NSRL-12478	Wood	901B-601A, 666.5-cm	9030 ± 60	10 139 ± 214	9914–10 246
	Lepúe tephra correlative (10 cm thick), 700 cm depth (basal contact)					
	ETH-20386	Bulk gyttja	901B-601A, 702 cm	9695 ± 90	10 982 ± 290	10 735–11 225
	ETH-18856	Wood	901B-601A, 706 cm	9415 ± 80	10 595 ± 286	10 289–11 063
	AA23236	Wood	901B-601A, 706 cm	9635 ± 85	10 938 ± 284	10 696–11 196
	ETH-188857	Bulk gyttja	901B-601A, 710 cm	9545 ± 70	10 820 ± 308	10 580–11 100
	ETH-24476	Bulk gyttja	901B-601A, 712 cm	9830 ± 75	11 208 ± 244	10 800–11 399
Lago Condorito (Moreno, 2004)	A8070	Bulk gyttja	PM10, 685–688 cm	9680 ± 85	10 967 ± 282	10 732–11 211
	A8069	Bulk gyttja	PM10, 710–713 cm	10 060 ± 80	11 527 ± 328	11 245–11 917
	Lepúe tephra correlative (27 cm thick), 726 cm depth (basal contact)					
	A8068	Bulk gyttja	PM10, 821–824 cm	11 265 ± 65	13 090 ± 148	12 928–13 258
Laguna Tahui (Abarzúa *et al.*, 2004)	GX28215		004D, 891–895 cm	8990 ± 110	10 029 ± 332	9635–10 367
	Lepúe tephra correlative (16 cm thick), 932 cm depth (basal contact)					
	NSRL-12473	Bulk gyttja	004D, 934–936 cm	10 150 ± 50	11 703 ± 296	11 403–11 960
Lago Meli (Abarzúa and Moreno, 2008)		Terrestrial macrofossil	818–819 cm	9105 ± 70	10 227 ± 218	9930–10 479
	Lepúe tephra correlative (11 cm thick), 843 cm depth (basal contact)					
	CAMS-115814	Bulk gyttja	844 cm	10 000 ± 40	11 377 ± 218	11 247–11 610
Lago Lepúe (Pesce and Moreno, 2014)	ETH-25451	Bulk gyttja	0201 DT8, 786 cm	8965 ± 65	10 033 ± 234	9781–10 227
	Lepúe Tephra (44 cm thick), 870 cm depth (basal contact)					
	CAMS-125915	Bulk gyttja	0201 DT9, 904 cm	10 360 ± 40	12 123 ± 272	11 948–12 401
Offshore						
ODP Site 1233D (Lamy *et al.*, 2004)	KIA 21 451	Mixed planktonic foraminifera	12.94 mcd	9, 340 ± 80	10 175 ± 288	9916–10 387
	Lepúe Tephra (12 cm thick), 14.80 mcd (basal contact)					
	KIA21473	Mixed planktonic foraminifera	17.01 mcd	10 800 ± 70	12 276 ± 280	12 019–12 534

*Highest Probability Density Function Radiocarbon laboratories used in this study: UCIAMS, University of California at Irving AMS Facility; LLNL, Lawrence Livermore National Laboratory.
†The Southern Hemisphere terrestrial calibration curve (SHCal13) and OxCal Program (v. 4.2.4) were used for all samples.

and glacial diamicts (till). The morphological expression of Lepué Tephra within andic cover-bed sections of Isla Grande de Chiloé can be highly variable depending on the thickness of encapsulating andic material and the permeability of the underlying substrate. Where Lepué Tephra occurs within thin andic soil material closely overlying impermeable glacial diamicts (which seasonally perches the local water table), tephra color is strongly altered to strong brown chromas (i.e. Queilen and Chonchi sections, Fig. 11), whereas Lepué Tephra overlain by a thicker interval of free-draining andic soil material typically has gray to pale brown chromas (i.e. Lago Natri, Castro, Puente Puntra and Chacao sections, Fig. 11). In northern sections (i.e. Huelmo and along Ruta 5 connecting Pargua with Puerto Montt; Figs 10 and 12) Lepué Tephra is closely underlain by intensely weathered andesitic ash and lapilli 'ghosts' that are probably sourced from either Volcán Calbuco or Volcán Yate located eastwards along the Andean mountain divide. These highly weathered tephras have yet to be geochemically characterized.

Copyright © 2017 John Wiley & Sons, Ltd.

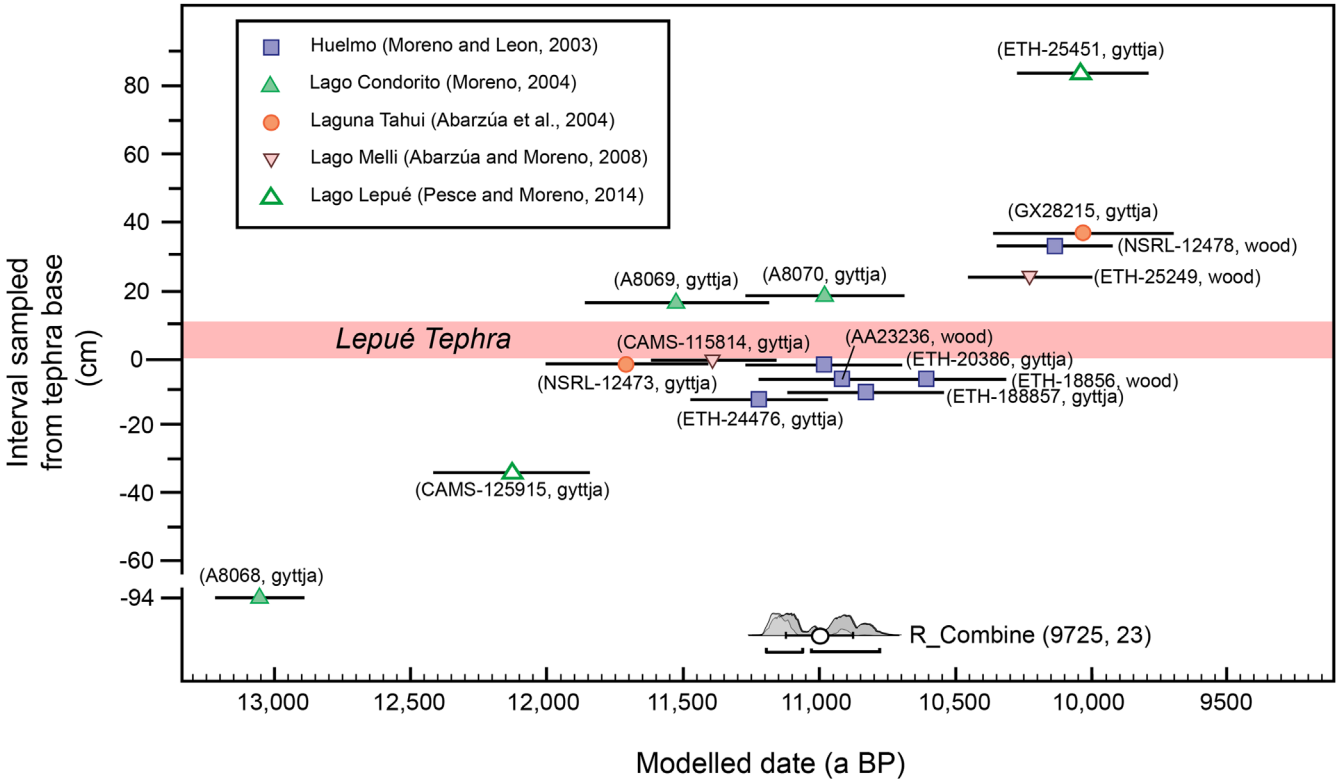

Figure 16. Modeled age determinations of Lepué Tephra from Huelmo mire (Moreno and León, 2003), L. Condorito (Moreno, 2004), L. Tahui (Abarzúa *et al.*, 2004), L. Melli (Abarzúa and Moreno, 2008) and L. Lepué (Pesce and Moreno, 2014). Modeled ages are arranged according to intervals (cm) sampled with respect to the basal contact of Lepué Tephra. Error bars represent $\pm 2\sigma$. A weighted mean modeled age determination of 9725 ± 23 ^{14}C a BP for Lepué Tephra is based on eight R-combine-statistically grouped samples from Huelmo mire (ETH-20386), L. Condorito (A8069), L. Tahui (NSRL-12473 and GX28215), L. Melli (ETH-25249) and L. Lepué (CAMS-125915 and ETH-25451). The associated mean age of $10\,994 \pm 124$ cal a BP is indistinguishable from a mean age of $10\,909 \pm 228$ cal a BP determined for Lepué Tephra from Chaitén (S-4, S-12A), Puelche and Pichileufú (this study; Fig. 5).

Lake records

A large number of cores over many years have been retrieved from bogs (Heusser and Heusser, 2006; Heusser *et al.*, 2006) and shallow lakes throughout north-western Patagonia to elucidate vegetation–climate change, fire regime shifts and volcanic disturbance (i.e. Moreno and León, 2003; Pesce and Moreno, 2014; Henríquez *et al.*, 2015). A key priority for these ongoing investigations has been to disentangle the role of paleofires and explosive volcanism from climate drivers of past vegetation change. Until recently, the occurrence of Lepué Tephra has been a subordinate focus in dominantly paleoecologically directed investigations. However, there is growing appreciation of the utility this tephra is able to play in terms of vegetation–climate synchronization within equivalent-aged lake records of diverse latitude and elevation.

Lepué Tephra can be readily identified in most sediment cores as a macroscopic layer (cm thick) showing primary fall deposition with minimal post-depositional reworking. However, in some lakes (i.e. Lago Lepué; Pesce and Moreno, 2014) Lepué Tephra shows evidence of reworking and is substantially over-thickened compared with adjacent lake sequences. In all cases, Lepué Tephra can be readily identified as a very prominent down-core inorganic density (g ml^{-1}) peak (Fig. 13). For cores throughout Isla Grande de Chiloé [i.e. Lago (L.) Quilque, L. Tarumán, L. Lepué, L. Melli and L. Tahui] this peak occurs at ~ 750 cm depth with a subordinate inorganic peak at ~650 cm probably representing a VCha-sourced tephra, which is not typically expressed macroscopically in adjacent andic soil cover-beds (Alloway *et al.*, 2017). For continental cores south of Puerto Montt (i.e. L. Condorito, Huelmo mire, L. El Salto), Lepué Tephra occurs at ~650 cm depth, whereas at L. Proschle and Puelche Section Lepué Tephra occurs at ~350 cm depth, and is associated with minor inorganic spikes probably representing tephra additions from Volcán (V.) Chaitén, V. Apagado and V. Calbuco. In all lake cores throughout the region, the ages of Lepué Tephra are well constrained by numerous radiocarbon dates (see Age Section below).

So far the northernmost occurrence of Lepué Tephra within lake sediments is found at Lago Pichilaguna, located immediately west of Llanquihue township and ~178 km north-west of V. Michimahuida. Here, Lepué Tephra occurs at 382–390 cm depth within core 1402AT3 as an ~8-cm-thick dark olive-gray, normal graded coarse to very fine ash (see photo inset Fig. 10) and is chronologically constrained by bracketing radiocarbon dates of 8905 ± 35 ^{14}C a BP (CAMS-158137; 9989 ± 113 cal a BP) above and $10\,100 \pm 25$ ^{14}C a BP (UCIAMS-177595; $11\,576 \pm 109$ cal a BP) below. In this same vicinity, Lepué Tephra is not macroscopically preserved within the andic soil-forming environment.

In lakes close to its presumed Michimahuida source, only sediments and tephra post-dating Lepué Tephra have been retrieved since it forms a prominent hardpan and a significant obstacle for further core penetration. For example, at Lago Teo located near Chaitén (Moreno *et al.*, 2015a), no core penetration beyond 3.02 m depth was achieved. Lepué Tephra was not encountered despite being prominently expressed in all adjacent road sections. An age of 8925 ± 30 ^{14}C a BP of organic sediments from the base of the Lago Teo core provides a minimum age of 10 021 cal a BP for Lepué Tephra in this sector.

Offshore record

Site 1233 was drilled during ODP Leg 202 off southern continental Chile (41°0.01′S, 74°26.99′W; 40 km offshore;

Copyright © 2017 John Wiley & Sons, Ltd.

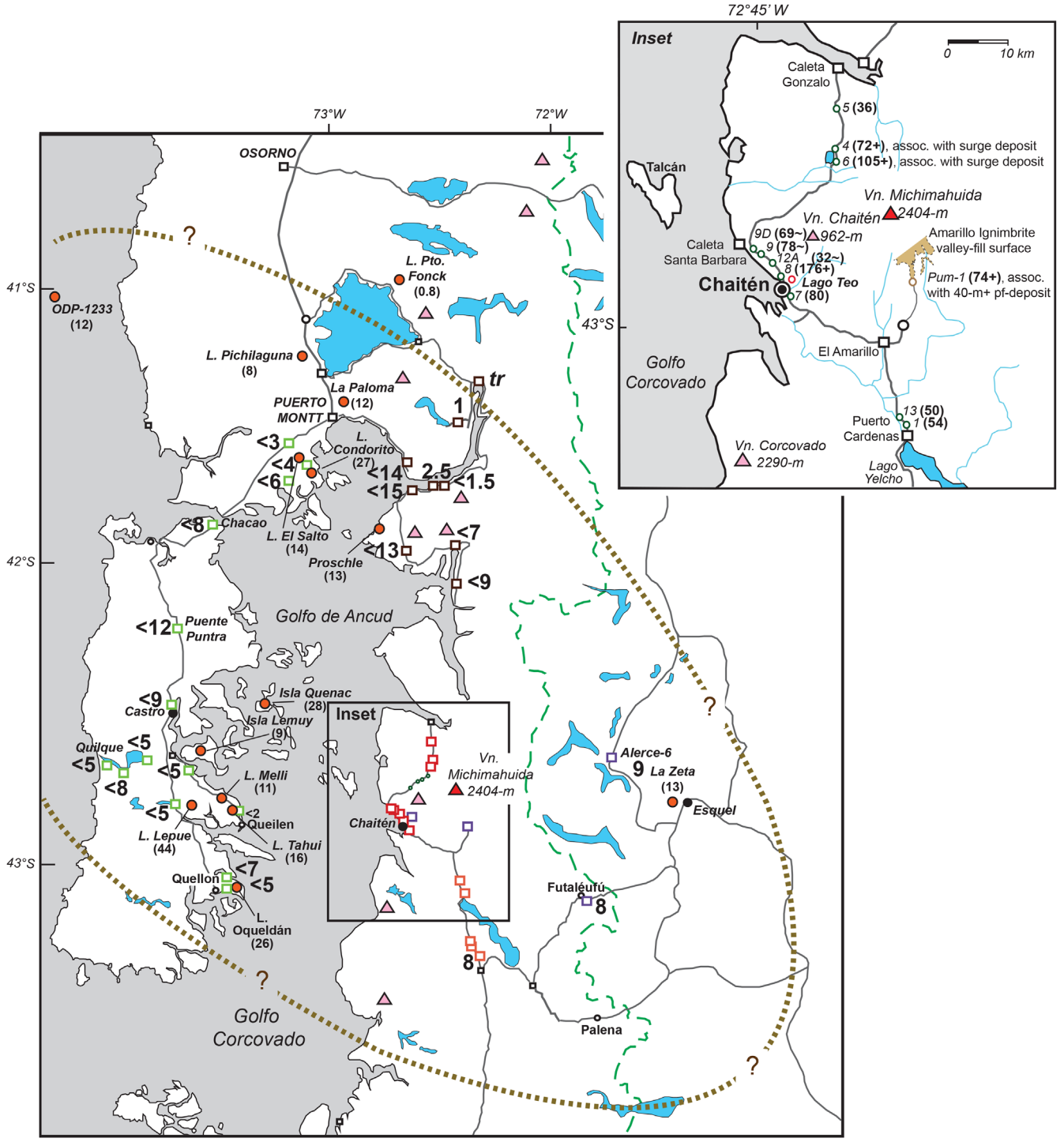

Figure 17. Map of the study area indicating the maximum recorded thicknesses (cm) of Lepué Tephra occurring within andic soil cover-bed sections. At any one site, it is usually very difficult to derive a representative thickness for the pocketed, highly irregular and variably thick Lepué Tephra. Thickness values from lake cores are also shown and indicate considerable thickness differences between adjacent soil and lacustrine depositional environments. Large thickness variations were also noted between closely situated closed basin lakes, suggesting that either tephra thickness measurements made from previous studies may not have distinguished between primary and secondary tephric inputs or, perhaps, the existence of more complex sedimentary inputs to these lake systems.

838 m water depth) in a small basin on the upper continental slope away from the pathway of major turbidity currents. This offshore site is located at the northern margin of the Antarctic Circumpolar Current (ACC) and at the origin of the Perú–Chile Current (PCC), the most latitudinally extensive Eastern Boundary Current system in the world, driven by along-shore parallel winds along the Pacific coast of South America. This offshore core yielded high-resolution alkenone-based sea surface temperature (SST) and vegetation records extending over the last 50–70 000 years (Kaiser *et al.*, 2005, 2008; Heusser *et al.*, 2006; Lamy *et al.*, 2007). A prominent macroscopic tephra layer was registered in core 1233D within clay and silty clays between 14.52 and 14.83 meters composite depth (mcd) and was accompanied by a prominent spike in magnetic susceptibility [916.8 m mol^{-1} (SI)] (Fig. 14). Unfortunately, no radiocarbon dates were obtained directly associated with the upper and lower contacts of this tephra but bracketing radiocarbon samples from 12.94 and 17.01 mcd yielded calibrated ages of 10 040 and 12 260 cal a BP, respectively.

Copyright © 2017 John Wiley & Sons, Ltd.

Table 2. Summary of individual glass shard major-element compositions (normalized to an anhydrous basis) of proximal to distal Lepué Tephra in the Chaitén, Isla Grande de Chiloé and Esquel sectors of NW Patagonia.

Sample	Probe run	Sample no.	SiO_2	Al_2O_3	TiO_2	FeO	MgO	MnO	CaO	Na_2O	K_2O	Cl	H_2O	*n*
Microlite-poor glass														
Section 4	*19 April 2013*	13-06-32-1	71.09	14.30	0.34	3.92	0.25	0.14	1.30	4.95	3.51	0.19	−1.04	
Paso de Lago		13-06-32-2	71.27	14.24	0.39	3.72	0.28	0.13	1.45	4.89	3.43	0.20	−0.62	
Blanco		13-06-32-3	71.29	14.25	0.28	3.75	0.21	0.16	1.40	4.99	3.48	0.17	−0.77	
14J13S4-2		13-06-32-6	71.53	14.34	0.33	3.30	0.20	0.12	1.31	5.22	3.47	0.19	−0.10	
		13-06-32-7	71.24	14.33	0.33	3.63	0.20	0.13	1.33	5.14	3.48	0.19	−0.74	
		13-06-32-8	71.28	14.18	0.32	3.81	0.20	0.11	1.27	5.03	3.61	0.20	−1.16	
		13-06-32-9	71.44	14.22	0.31	3.43	0.21	0.13	1.30	5.23	3.56	0.18	−1.58	
		13-06-32-10	71.04	14.26	0.40	3.65	0.23	0.11	1.40	5.18	3.55	0.19	−0.77	
		13-06-32-11	70.91	14.23	0.33	3.94	0.22	0.15	1.41	5.23	3.38	0.20	−1.26	
		13-06-32-12	71.32	14.19	0.31	3.75	0.25	0.13	1.43	4.84	3.60	0.19	−0.01	
		13-06-32-13	70.87	14.15	0.35	3.84	0.28	0.13	1.43	5.06	3.70	0.19	−0.79	
		13-06-32-14	71.12	14.13	0.41	3.59	0.25	0.14	1.45	5.14	3.59	0.18	−0.63	
		13-06-32-15	71.83	14.16	0.31	3.45	0.18	0.15	1.30	4.88	3.57	0.17	−0.57	
		13-06-32-16	71.23	13.95	0.37	3.87	0.19	0.16	1.44	4.97	3.62	0.20	−0.82	
		13-06-32-17	71.31	14.20	0.37	3.68	0.20	0.13	1.35	5.02	3.53	0.20	−0.90	
		13-06-32-18	71.60	13.97	0.35	3.72	0.20	0.17	1.33	4.96	3.50	0.19	−1.33	
		13-06-32-19	70.62	14.12	0.35	3.89	0.30	0.18	1.50	5.39	3.49	0.17	−1.77	
		13-06-32-20	71.21	14.18	0.35	3.71	0.21	0.18	1.36	4.99	3.62	0.19	−0.34	
Average			***71.23***	***14.19***	***0.34***	***3.70***	***0.23***	***0.14***	***1.38***	***5.06***	***3.54***	***0.19***	***−0.84***	***18***
SD			***0.28***	***0.10***	***0.03***	***0.18***	***0.03***	***0.02***	***0.07***	***0.15***	***0.08***	***0.01***	***0.46***	
Section 5	*19 April 2013*	13-06-35-1	71.19	14.01	0.37	3.90	0.23	0.14	1.34	5.03	3.59	0.21	−0.20	
Puente Aguila		13-06-35-2	71.16	14.22	0.33	3.83	0.20	0.15	1.33	5.04	3.54	0.20	−2.32	
14J13S5-1		13-06-35-3	72.13	13.84	0.33	3.52	0.15	0.17	1.14	4.85	3.67	0.20	0.71	
		13-06-35-4	70.78	14.37	0.36	3.89	0.28	0.14	1.51	5.09	3.40	0.19	−1.97	
		13-06-35-5	71.44	14.17	0.34	3.76	0.23	0.08	1.36	4.88	3.54	0.19	−1.20	
		13-06-35-6	71.73	14.12	0.29	3.52	0.20	0.14	1.35	4.92	3.56	0.18	−0.68	
		13-06-35-7	71.42	14.09	0.29	3.73	0.19	0.16	1.32	4.98	3.63	0.20	0.06	
		13-06-35-8	71.21	14.11	0.29	3.92	0.19	0.18	1.35	5.08	3.49	0.18	−1.71	
		13-06-35-9	70.18	14.51	0.43	4.07	0.31	0.15	1.68	5.20	3.33	0.15	−2.58	
		13-06-35-10	71.20	14.16	0.34	3.83	0.23	0.14	1.35	4.91	3.67	0.17	−2.01	
		13-06-35-13	71.13	14.19	0.33	3.65	0.17	0.16	1.38	5.20	3.59	0.21	−1.30	
		13-06-35-14	71.49	14.17	0.29	3.70	0.18	0.15	1.36	4.89	3.56	0.21	−0.87	
		13-06-35-15	71.43	14.22	0.34	3.62	0.22	0.12	1.38	4.56	3.92	0.19	−0.48	
		13-06-35-16	71.68	14.03	0.32	3.70	0.19	0.12	1.34	4.93	3.50	0.20	0.01	
		13-06-35-17	71.12	14.28	0.34	3.78	0.20	0.12	1.32	5.12	3.54	0.17	−2.47	
		13-06-35-18	71.83	13.90	0.32	3.47	0.17	0.14	1.25	5.08	3.69	0.16	−1.31	
Average			***71.32***	***14.15***	***0.33***	***3.74***	***0.21***	***0.14***	***1.36***	***4.98***	***3.58***	***0.19***	***−1.14***	***16***
SD			***0.45***	***0.16***	***0.04***	***0.16***	***0.04***	***0.02***	***0.11***	***0.16***	***0.13***	***0.02***	***1.00***	
La Zeta, Esquel	*16 July 2012*	12-05-29_2	71.41	13.96	0.31	3.89	0.20	0.15	1.27	5.07	3.55	0.20	−1.85	
LAZ-T7B		12-05-29_4	70.97	14.28	0.32	3.88	0.17	0.15	1.27	5.19	3.55	0.20	−1.16	
		12-05-29_7	71.53	13.90	0.36	3.76	0.22	0.17	1.33	4.97	3.52	0.24	0.38	
		12-05-29_8	71.12	14.11	0.34	3.76	0.21	0.14	1.24	5.32	3.56	0.21	−0.25	
		12-05-29_9	71.48	14.31	0.31	3.81	0.21	0.11	1.27	4.96	3.34	0.21	−0.27	
		12-05-29_10	71.13	14.37	0.31	3.70	0.20	0.15	1.27	5.12	3.55	0.20	−0.98	
		12-05-29_12	71.53	14.19	0.31	3.54	0.19	0.16	1.33	5.02	3.52	0.21	−0.24	
		12-05-29_13	71.03	14.32	0.36	3.73	0.20	0.13	1.33	5.25	3.47	0.19	−0.64	
		12-05-29_15	71.00	14.19	0.33	3.79	0.19	0.10	1.29	5.25	3.63	0.22	−0.56	
		12-05-29_17	71.19	14.24	0.32	3.90	0.20	0.15	1.39	4.86	3.54	0.21	0.77	
		12-05-29_18	69.91	15.82	0.26	2.97	0.12	0.12	1.89	5.73	3.02	0.17	1.33	
		12-05-29_22	71.38	13.87	0.33	3.99	0.19	0.15	1.47	6.50	1.92	0.21	0.98	
Average			***71.14***	***14.30***	***0.32***	***3.73***	***0.19***	***0.14***	***1.36***	***5.27***	***3.35***	***0.21***	***−0.21***	***12***
SD			***0.44***	***0.51***	***0.03***	***0.27***	***0.02***	***0.02***	***0.18***	***0.45***	***0.48***	***0.02***	***0.93***	
La Zeta, Esquel	*16 July 2012*	12-05-28_1	71.82	14.08	0.33	3.58	0.17	0.17	1.20	4.71	3.70	0.24	3.68	
LAZ-T7A		12-05-28_2	71.50	14.08	0.31	3.78	0.21	0.16	1.26	4.90	3.61	0.21	−0.81	
		12-05-28_3	70.81	14.32	0.34	3.86	0.22	0.15	1.32	5.34	3.44	0.21	−0.35	
		12-05-28_4	71.17	14.30	0.32	3.76	0.20	0.14	1.31	4.96	3.63	0.21	0.61	
		12-05-28_5	70.90	14.30	0.33	3.67	0.19	0.16	1.36	5.32	3.59	0.20	−1.21	
		12-05-28_7	71.34	14.14	0.34	3.67	0.19	0.13	1.28	5.10	3.61	0.20	2.80	
		12-05-28_8	70.91	14.35	0.32	3.58	0.20	0.17	1.30	5.20	3.77	0.20	−1.63	
		12-05-28_9	71.48	14.13	0.33	3.73	0.18	0.15	1.26	4.87	3.68	0.19	−0.36	
		12-05-28_10	71.28	14.52	0.33	3.75	0.22	0.11	1.32	4.71	3.56	0.19	−0.81	
		12-05-28_11	71.81	13.85	0.36	3.66	0.19	0.15	1.20	5.01	3.55	0.22	−1.02	
		12-05-28_12	71.46	14.24	0.32	3.60	0.17	0.15	1.25	4.99	3.59	0.22	−0.84	
		12-05-28_13	71.73	14.19	0.32	3.55	0.19	0.15	1.26	4.83	3.59	0.19	−0.38	
		12-05-28_14	71.40	13.99	0.33	3.81	0.19	0.16	1.26	5.05	3.61	0.20	−0.61	
		12-05-28_16	71.46	14.02	0.34	3.73	0.22	0.14	1.32	5.04	3.51	0.23	0.20	

continued

Copyright © 2017 John Wiley & Sons, Ltd.

Table 2. (*Continued*)

Sample	Probe run	Sample no.	SiO_2	Al_2O_3	TiO_2	FeO	MgO	MnO	CaO	Na_2O	K_2O	Cl	H_2O	*n*
		12-05-28_17	71.27	14.23	0.35	3.71	0.19	0.14	1.29	5.06	3.58	0.20	−0.44	
		12-05-28_18	71.52	13.91	0.33	3.69	0.20	0.13	1.27	5.19	3.55	0.20	−0.85	
		12-05-28_19	71.59	14.18	0.32	3.58	0.21	0.15	1.26	4.88	3.64	0.19	−0.77	
		12-05-28_20	71.47	14.25	0.32	3.63	0.22	0.14	1.31	4.85	3.61	0.20	−0.06	
Average			***71.38***	***0.33***	***14.17***	***3.68***	***0.15***	***0.20***	***1.28***	***5.00***	***3.60***	***0.21***	***−0.16***	***18***
SD			***0.29***	***0.01***	***0.17***	***0.09***	***0.01***	***0.01***	***0.04***	***0.18***	***0.07***	***0.01***	***1.35***	
ODP-1233	*26 August 2014*	14-01_06-1	70.61	14.70	0.41	3.83	0.30	0.16	1.72	4.66	3.45	0.17	1.71	
14.68-m		14-01_06-4	71.20	14.05	0.30	3.79	0.24	0.16	1.49	5.18	3.50	0.08	−1.47	
		14-01_06-11	71.09	14.36	0.33	3.89	0.21	0.17	1.47	4.81	3.57	0.09	0.52	
		14-01_06-13	71.05	14.40	0.36	3.88	0.25	0.17	1.42	4.86	3.54	0.09	−0.42	
		14-01_06-16	71.42	14.32	0.34	3.63	0.20	0.14	1.35	4.92	3.59	0.09	1.84	
Average			***71.07***	***14.36***	***0.35***	***3.81***	***0.24***	***0.16***	***1.49***	***4.89***	***3.53***	***0.10***	***0.44***	***5***
SD			***0.30***	***0.23***	***0.04***	***0.11***	***0.04***	***0.01***	***0.14***	***0.19***	***0.06***	***0.04***	***1.41***	
Microlitic glass														
ODP-1233	*26 August 2014*	14-01_06-2	56.18	14.89	2.06	9.83	4.25	0.21	7.42	3.54	1.53	0.08	0.77	
14.68-m		14-01_06-3	55.88	15.39	1.88	9.69	4.14	0.19	7.64	3.55	1.44	0.21	2.35	
		14-01_06-5	58.69	16.60	1.76	8.04	2.61	0.18	6.01	4.41	1.65	0.06	0.49	
		14-01_06-6	55.89	15.41	2.02	9.77	4.05	0.18	7.50	3.62	1.45	0.10	1.37	
		14-01_06-7	64.93	20.82	0.12	1.51	0.08	0.04	3.99	6.92	1.50	0.09	−0.39	
		14-01_06-8	63.31	19.33	0.52	3.60	0.59	0.08	5.37	5.18	1.94	0.09	1.63	
		14-01_06-9	55.90	15.87	1.82	9.15	4.09	0.13	7.63	3.85	1.37	0.20	1.02	
		14-01_06-10	56.47	15.51	2.06	9.55	3.83	0.15	7.32	3.37	1.54	0.19	2.20	
		14-01_06-12	62.07	22.54	0.20	1.42	0.17	0.06	5.48	6.84	1.04	0.19	0.08	
		14-01_06-14	56.06	15.39	2.01	9.92	4.02	0.19	7.43	3.44	1.44	0.10	1.45	
		14-01_06-15	55.84	15.56	2.03	9.67	4.30	0.20	7.87	3.16	1.28	0.09	2.97	
		14-01_06-17	56.25	15.14	2.11	10.00	4.14	0.22	7.27	3.36	1.49	0.03	0.15	
		14-01_06-18	56.15	19.34	1.60	7.13	2.05	0.15	8.12	4.24	1.15	0.08	3.89	
		14-01_06-19	66.34	17.65	0.33	3.21	0.48	0.08	3.45	6.01	2.35	0.11	−1.06	
		14-01_06-20	56.12	15.64	2.04	9.30	4.20	0.18	7.72	3.28	1.39	0.14	2.67	
		14-01_06-21	56.03	15.47	2.04	9.57	4.23	0.21	7.27	3.62	1.48	0.08	−0.12	
		14-01_06-22	62.57	22.77	0.07	1.02	0.03	0.02	5.12	7.47	0.83	0.10	−0.64	
		14-01_06-23	56.10	15.38	2.03	9.71	4.07	0.16	7.54	3.52	1.40	0.10	0.89	
		14-01_06-24	67.82	18.26	0.22	2.44	0.13	0.09	3.21	5.75	2.05	0.03	0.77	
		14-01_06-25	65.80	13.52	1.60	7.16	1.01	0.18	2.86	4.11	3.65	0.10	1.50	
Average			***59.22***	***17.02***	***1.43***	***7.09***	***2.62***	***0.14***	***6.31***	***4.46***	***1.60***	***0.11***	***1.10***	***20***
SD			***4.33***	***2.63***	***0.81***	***3.42***	***1.80***	***0.06***	***1.74***	***1.38***	***0.59***	***0.05***	***1.28***	
Lago Lepué	*23 October 2012*	12-17-1-1	55.52	15.28	1.81	9.50	4.62	0.17	7.37	4.23	1.50	*n.d*	−0.68	
Chiloé		12-17-1-2	55.55	16.00	1.72	9.88	3.60	0.18	6.84	4.76	1.46	*n.d*	−1.37	
		12-17-1-3	54.22	16.19	1.84	9.99	4.28	0.23	7.17	4.85	1.23	*n.d*	−0.45	
		12-17-1-9	55.65	15.19	1.85	9.67	4.32	0.18	7.16	4.42	1.56	*n.d*	−0.85	
		12-17-1-11	55.83	15.21	1.81	9.52	4.46	0.17	7.11	4.33	1.56	*n.d*	−1.06	
		12-17-1-12	54.70	16.32	1.85	10.08	4.07	0.21	7.25	4.19	1.32	*n.d*	−1.62	
		12-17-1-13	56.72	15.98	1.59	9.11	3.39	0.21	6.32	4.99	1.69	*n.d*	0.06	
		12-17-1-17	54.32	15.52	2.03	10.61	4.35	0.20	7.29	4.43	1.26	*n.d*	−0.68	
Average			***55.31***	***15.71***	***1.81***	***9.80***	***4.14***	***0.19***	***7.06***	***4.53***	***1.45***		***−0.83***	***16***
SD			***0.85***	***0.46***	***0.12***	***0.45***	***0.43***	***0.02***	***0.34***	***0.30***	***0.16***		***0.53***	
Pumalin-4	*19 April 2013*	13-03-13-1	54.11	15.44	2.30	10.40	4.28	0.24	7.64	3.89	1.59	0.11	0.54	
		13-03-13-2	54.41	15.34	2.36	10.39	4.24	0.16	7.65	3.82	1.53	0.10	0.58	
		13-03-13-3	53.77	15.42	2.41	10.57	4.17	0.18	7.79	4.01	1.58	0.10	0.53	
		13-03-13-4	55.13	15.63	1.73	8.61	4.77	0.20	6.94	2.69	4.26	0.03	0.31	
		13-03-13-5	56.71	16.38	1.68	9.28	3.22	0.18	6.58	4.28	1.57	0.12	0.95	
Average			***54.82***	***15.64***	***2.10***	***9.85***	***4.14***	***0.19***	***7.32***	***3.74***	***2.11***	***0.09***	***0.58***	***5***
SD			***1.17***	***0.43***	***0.36***	***0.86***	***0.56***	***0.03***	***0.53***	***0.61***	***1.20***	***0.03***	***0.23***	
Section 4	*19 April 2013*	13-06-33-1	67.66	15.14	0.67	4.92	0.76	0.15	2.51	5.10	2.96	0.14	−0.83	
Paso de Lago		13-06-33-2	66.70	15.37	0.68	5.54	0.76	0.13	2.51	5.23	2.86	0.22	0.84	
Blanco		13-06-33-3	70.76	14.36	0.37	3.67	0.24	0.22	1.52	5.03	3.66	0.18	−2.50	
14J13S4-3		13-06-33-4	70.59	14.14	0.42	4.05	0.27	0.12	1.63	4.94	3.65	0.19	−2.69	
		13-06-33-5	65.07	14.72	0.78	6.08	1.24	0.22	3.47	5.51	2.74	0.18	−2.55	
		13-06-33-6	67.12	15.01	0.63	5.26	0.91	0.18	2.57	5.06	3.13	0.13	−2.32	
		13-06-33-7	68.99	14.65	0.52	4.54	0.68	0.19	2.13	4.92	3.26	0.13	−2.43	
		13-06-33-8	65.60	14.56	0.68	5.00	0.62	0.22	5.15	4.95	3.04	0.18	0.44	
		13-06-33-9	71.25	14.21	0.36	3.95	0.21	0.08	1.43	5.01	3.32	0.18	−1.94	
		13-06-33-10	71.07	14.02	0.34	3.81	0.21	0.15	1.35	5.34	3.50	0.20	−2.45	
		13-06-33-12	69.53	14.43	0.48	4.53	0.56	0.19	1.96	4.86	3.33	0.14	−2.05	
		13-06-33-13	70.77	14.37	0.34	3.80	0.34	0.12	1.71	4.96	3.41	0.17	−1.73	
		13-06-33-14	69.39	14.58	0.53	4.54	0.54	0.13	2.07	4.67	3.38	0.17	−1.42	
		13-06-33-15	68.00	14.66	0.53	4.95	0.64	0.13	2.37	4.77	3.78	0.16	−2.61	
		13-06-33-16	71.54	13.97	0.30	3.67	0.14	0.09	1.29	5.17	3.65	0.20	−2.64	

continued

Copyright © 2017 John Wiley & Sons, Ltd.

Table 2. (*Continued*)

Sample	Probe run	Sample no.	SiO_2	Al_2O_3	TiO_2	FeO	MgO	MnO	CaO	Na_2O	K_2O	Cl	H_2O	*n*
		13-06-33-17	70.53	14.13	0.34	3.98	0.28	0.20	1.49	5.37	3.49	0.19	−3.03	
		13-06-33-18	70.52	14.35	0.34	3.85	0.26	0.19	1.51	5.18	3.60	0.20	−2.10	
Average			***69.12***	***14.51***	***0.49***	***4.48***	***0.51***	***0.16***	***2.16***	***5.06***	***3.34***	***0.17***	***−1.88***	***17***
SD			***2.06***	***0.39***	***0.15***	***0.72***	***0.30***	***0.04***	***0.96***	***0.22***	***0.31***	***0.03***	***1.09***	
			SiO_2	Al_2O_3	TiO_2	FeO	MgO	MnO	CaO	Na_2O	K_2O	Cl	Total	*n*
Glass Standard	*16 July 2012*	*Average*	75.57	12.20	0.25	3.32	0.10	0.10	1.70	3.78	2.64	0.05	99.71	*18*
ATHO-G		*SD*	0.48	0.08	0.02	0.15	0.02	0.01	0.05	0.15	0.10	0.01	0.58	
	23 October 2012		75.61	12.20	0.23	3.29	0.11	0.10	1.70	3.75	2.64	n.d.	99.63	*123*
			0.41	0.08	0.02	0.10	0.01	0.02	0.02	0.15	0.04		0.51	
	19 April 2013		75.61	12.20	0.24	3.27	0.09	0.11	1.70	3.73	2.64	0.04	99.63	*76*
			0.54	0.12	0.02	0.12	0.01	0.02	0.04	0.23	0.07	0.01	0.66	
	26 August 2014		75.62	12.20	0.26	3.27	0.09	0.10	1.70	3.73	2.64	0.04	99.66	*75*
			0.47	0.10	0.02	0.12	0.01	0.02	0.04	0.38	0.06	0.01	0.46	

Age

A weighted mean age determination of 9588 ± 20 ^{14}C a BP (95% probability: 10 080–10 714 cal a BP) was modeled for Lepué Tephra based on four R-combine-statistically grouped samples (UCIAMS-145938, LLNL-158290, LLNL-123032 and LLNL-12329) from Sections 4 and 12A, Pichileufú and Puelche, respectively (Fig. 15; Table 1). Three sample outliers from Sections 9 and 12A and Pumalín-1 (LLNL-158125, LLNL-158291 and LLNL-122960) were rejected. This modeled age of Lepué Tephra compares closely with a similarly modeled age of 9725 ± 23 ^{14}C a BP based on samples retrieved from Huelmo (Moreno and León, 2003), Lago (L.) Condorito (Moreno, 2004), L. Tahui (Abarzúa *et al.*, 2004), L. Melli (Abarzúa and Moreno, 2008) and L. Lepué (Pesce and Moreno, 2014) (Fig. 16; Table 1). The associated mean calendar age of $10\,994 \pm 124$ cal a BP collated from previous research is indistinguishable from a mean calendar age of $10\,909 \pm 228$ cal a BP determined for Lepué Tephra in this study from Chaitén (S-4, S-12A), Puelche and Pichileufú (Fig. 5).

Isopach

Lepué Tephra is extensively distributed from the Chaitén Section of southern Chile in a wide arc from Isla Grande de Chiloé in the west to Esquel, Argentina, across the Andes in the east (Fig. 17). Lepué Tephra can also be traced northwards to near Seno Reloncaví and immediately south of Puerto Montt. In routinely measuring the thickness of Lepué Tephra two problems are encountered. Thicknesses recorded in the soil-forming (andic) environment bear little resemblance to those determined from lake/peat records. We consider that the most accurate thicknesses are likely to be derived from lakes and organic-rich fens, although bedding characteristics need to be carefully scrutinized to distinguish between primary and secondary depositional features. For example, in L. Lepué (Pesce and Moreno, 2014) Lepué Tephra is recorded as being ~ 44 cm thick with this thickness being significantly at odds with those from adjacent cored lakes (i.e. L. Melli, 11 cm; L. Tahui, 16 cm), with no mention of bedding characteristics that might distinguish primary airfall products from secondary redeposition and reworking.

Within the andic soil environment Lepué Tephra typically forms a highly irregular and laterally intermittent layer of well-cemented ashy material. This lateral distribution is presumably coincident with the density and distribution of vegetation that probably existed at the time of deposition with continued biological disturbance since (i.e. interference by roots, tree-throw). At any one particular section within the Chaitén sector, thickness values for Lepué Tephra are highly variable and are, for the most part, interpreted as being over-thickened within the valleys and lower slopes adjacent to the Andean range-front (along which most roads follow). This pervasive over-thickening certainly restricts the production of a reliable isopach map and, by proxy, any accurate estimate of eruptive volume. However, these thickness measurement obstacles certainly do not diminish the utility of this tephra as one of the most important early Holocene stratigraphic markers in this sector.

Geochemistry

We report major and trace element chemistry of pumice and matrix glass from Lepué Tephra utilizing grain-discrete electron microprobe analysis (EMPA) and laser ablation inductively coupled plasma mass spectrometry (LA-ICP-MS) techniques (Table 2, Table S1 and Supporting Information Methods) as well as bulk solution nebulization ICP-MS (SN-ICP-MS) analyses (Table S2 and Supporting Information Methods). The key objective for this paper is to demonstrate its utility in supporting field correlations and is not intended to detail the genesis of the melt body (or melt bodies) involved. Thus, while a (micro)phenocryst assemblage dominated by plagioclase, with subordinate pyroxene and Fe–Ti oxide phases was noted, their routine analysis was not undertaken as mineral compositions, and their implications for petrogenesis of the deposit, were not considered central to this particular study. The grain-specific major and trace element characterization of the pure glass phase of the Lepué Tephra has proven to be difficult because of the progressive increase in the concentration of microphenocrysts (dominantly plagioclase) occurring within the tephra glass shards as the eruption proceeded.

Back-scatter electron (BSE) images of selected glass shards from Lepué Tephra correlatives indicate low microlite concentrations are observed within glassy grains at the base of the tephra sequence referred to as 'microlite-poor glass' which is broadly rhyolitic in composition (onset of the Lepué eruption; Fig. 18A–C). Higher up in the tephra sequence, the microlite concentration within the glassy grains increases significantly (Fig. 18D–F) giving 'intensely microlitic glass' which typically has a basaltic andesite composition. Analysing the intensely microlitic glass either by EMPA and/or by LA-ICP-MS is highly problematic in that microlites are inevitably included in the material analysed (i.e. Fig. 18G, H), even when using a 10-μm-diameter EMPA, or LA-ICP-MS, spot. However, with sufficient analyses, glass chemistry can be determined as an end-member to a trend of analyses

Copyright © 2017 John Wiley & Sons, Ltd.

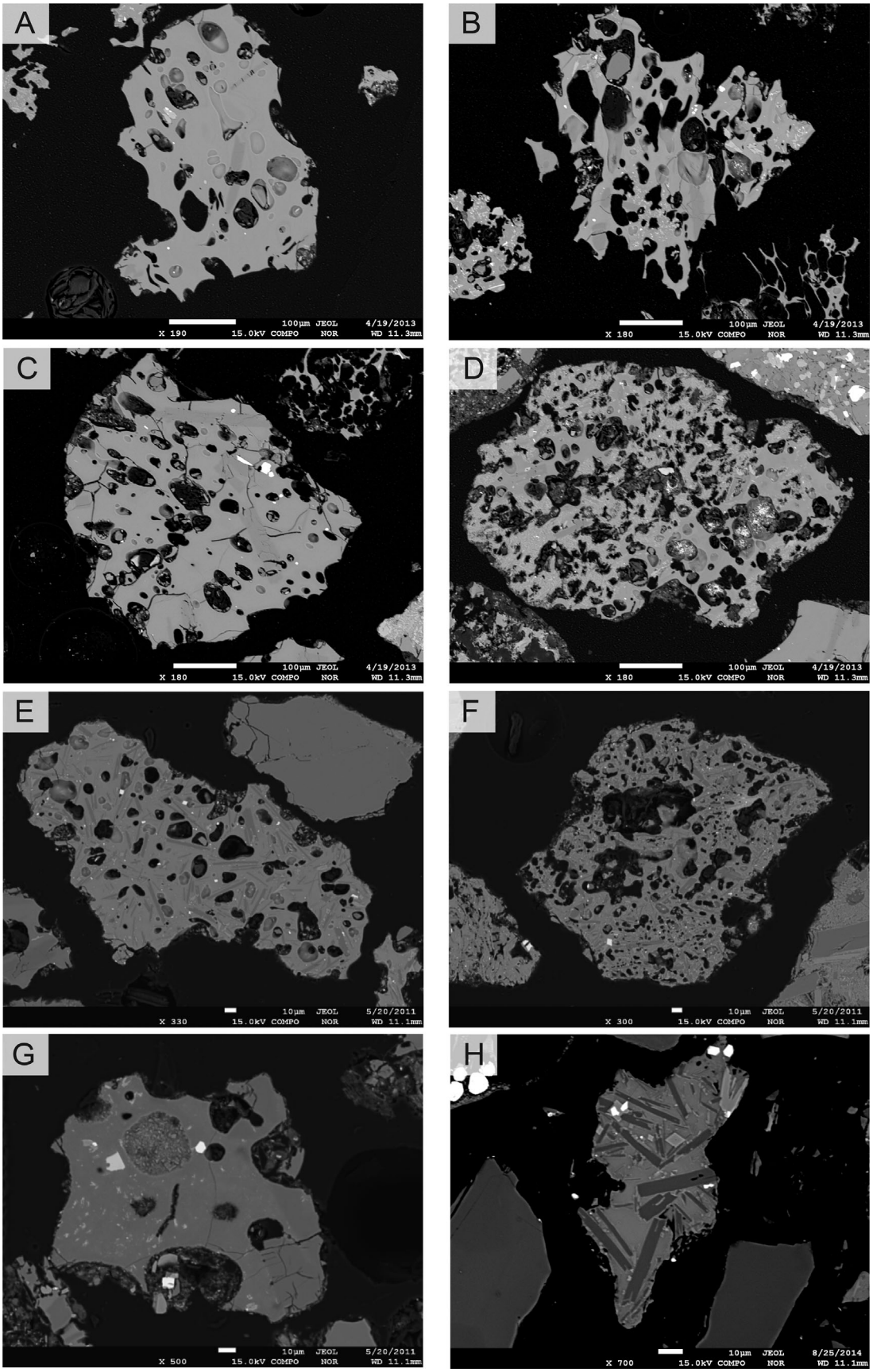

Figure 18. Selected back-scatter electron (BSE) images of glass shards from Lepué Tephra correlatives showing the varying concentration of dominantly plagioclase microlites within their glassy matrix (A, B – lowermost Lepué, Section 4; C – lowermost Lepué, Section 5; D – uppermost Lepué, Section 5; E –1819–1821 cm, L. Lepué; F –1831–1838 cm, L. Lepué; G – Lepué Tephra, Puente Puntra, Isla Grande de Chiloé; H –14.68 m, ODP-1233D). Low microlite concentrations were observed within glassy grains at the base of the tephra (onset of the Lepué eruption; A, B, C), but the microlite concentration within the matrix of glassy grains significantly increases (D, E, F) progressively upwards within the tephra deposit. In distal localities, the overwhelming dominance of glass grains containing profuse microlites made it very difficult and, in many cases, impossible for 10–20-µm-diameter electron and laser beams to be positioned on glass and without any obvious microlite contamination (i.e. G, H). Note that as the microlite concentration increases, the proportion of well-formed oriented vesicles decrease with a corresponding increase in irregular shaped (collapsed) and coalesced voids (D, F).

Copyright © 2017 John Wiley & Sons, Ltd.

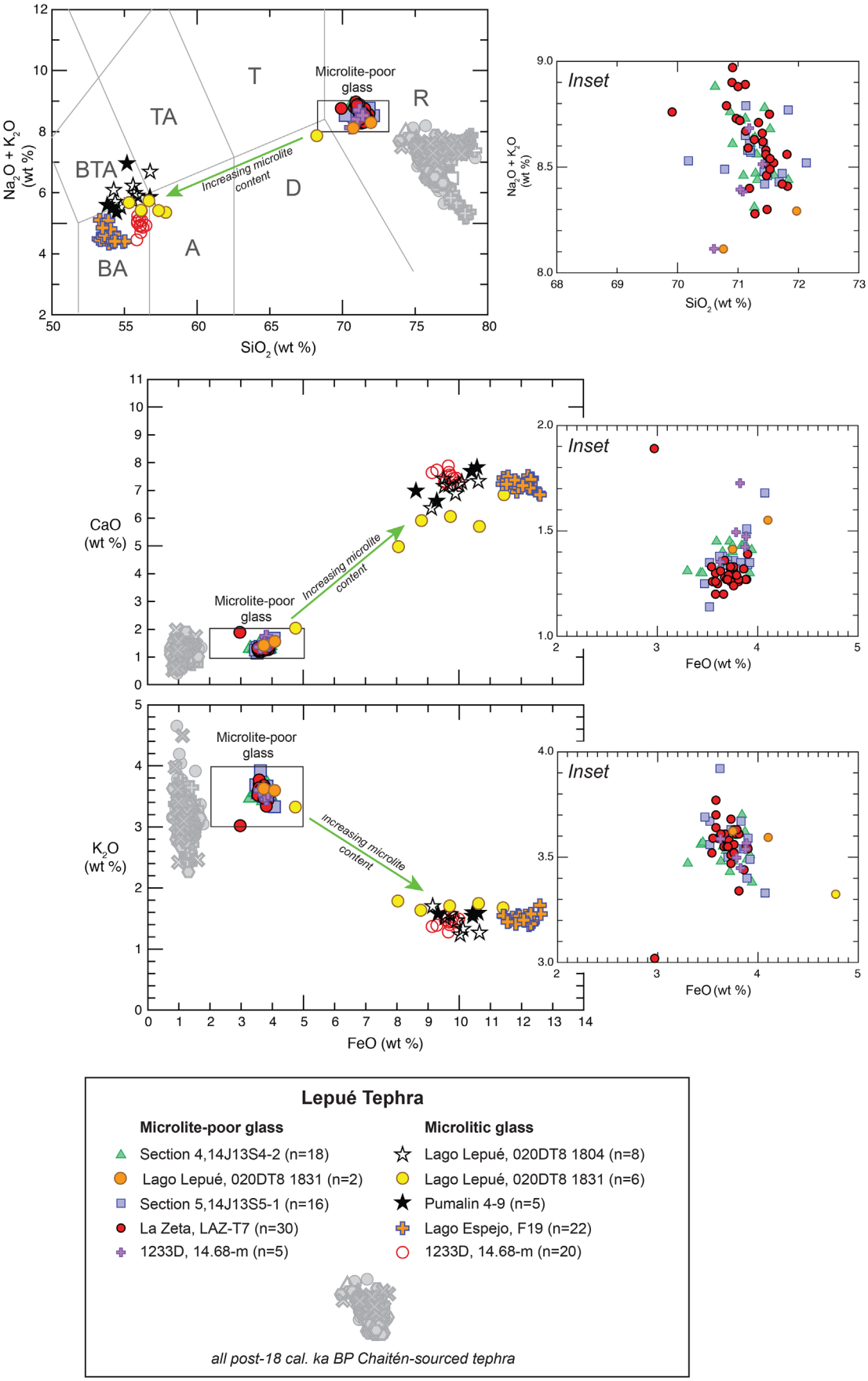

Figure 19. Selected major element compositions (weight per cent SiO_2 *vs.* $Na_2O + K_2O$ and FeO *vs.* K_2O and CaO) of glass shards from Lepué Tephra correlatives. Two glass end members, microlite-poor and microlitic, are plotted to show compositional and elemental concentration differences occurring between these two end members. All post-18 000 cal a BP Chaitén-sourced tephras are plotted for comparison.

Copyright © 2017 John Wiley & Sons, Ltd.

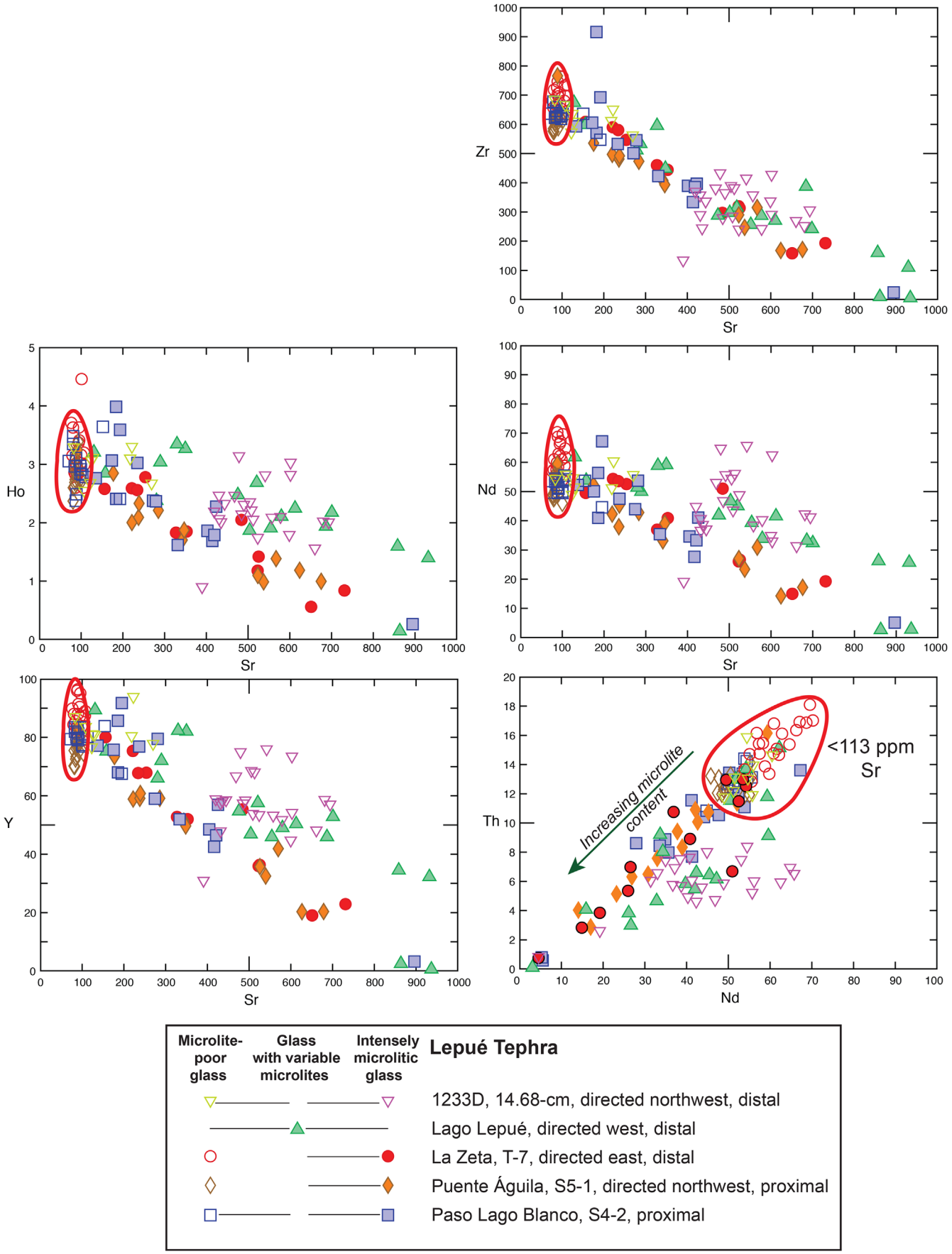

Figure 20. Nd *vs.* Th and Sr *vs.* Y, Ho, Nd, Zr compositions of glass shards from Lepué Tephra correlatives determined by grain discrete LA-ICP-MS analysis. Microlite-poor and microlitic glass data are plotted and show significant concentration differences between these two glass types associated with the ablation of (dominantly) plagioclase with glass. The microlite-poor glass compositions occur between 73 and 113 p.p.m. Sr, and these analyses are indicated on the plot of Nd *vs.* Th. See text for explanation.

Copyright © 2017 John Wiley & Sons, Ltd.

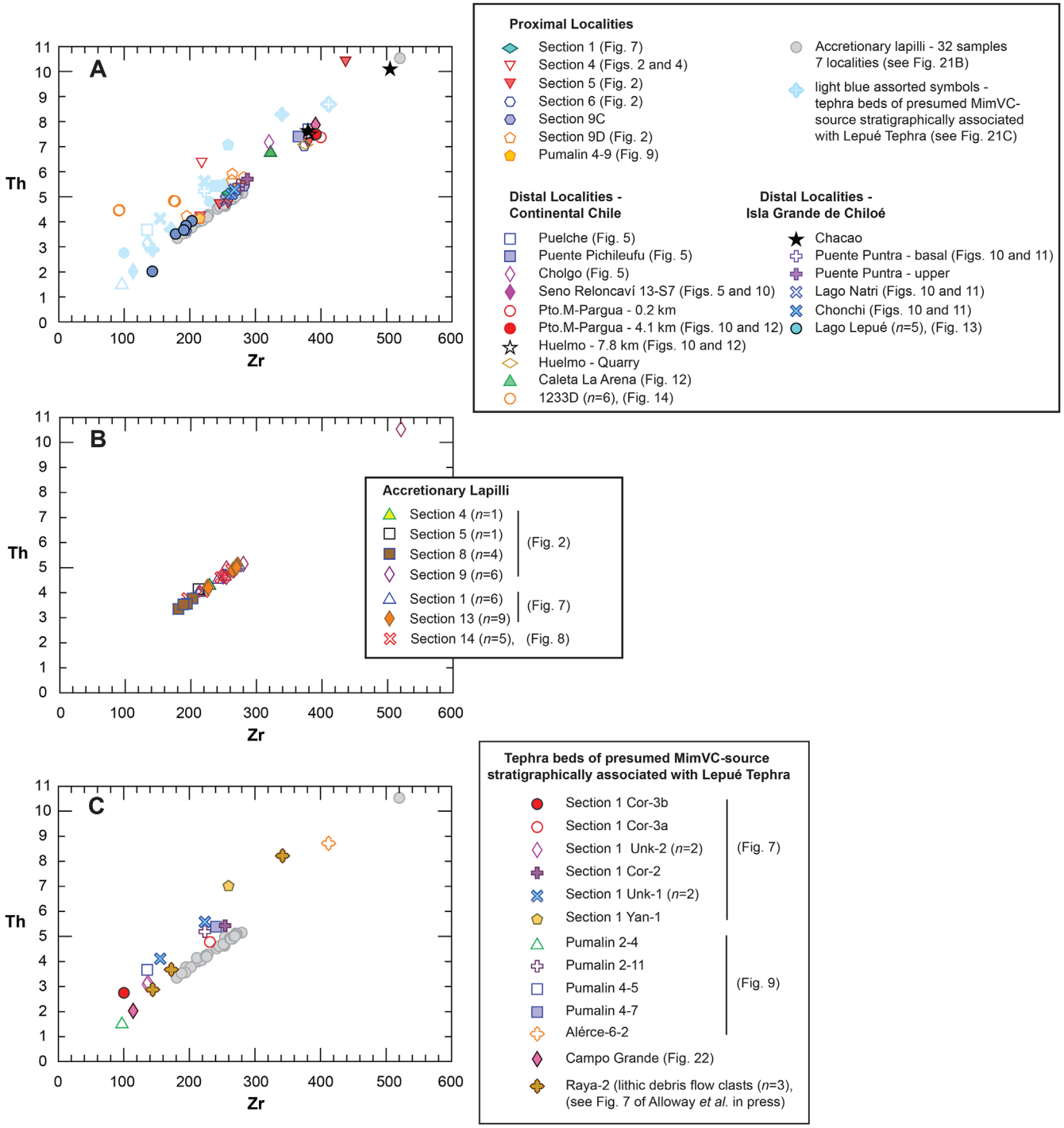

Figure 21. Th *vs.* Zr (p.p.m.) plots as determined by bulk sample solution ICP-MS analysis showing Lepué Tephra correlatives from proximal and distal sites (continental Chile and Isla Grande de Chiloé). These results are compared with individually analysed accretionary lapilli from seven proximal Lepué Tephra localities. Tephra beds of presumed MimVC source stratigraphically associated with Lepué Tephra are plotted for comparison.

contaminated by (dominantly) plagioclase phenocrysts, and in some cases 'microlite-free' analyses can be produced, particularly so from the microlite-poor glass shards. Coinciding with the increase in microlite concentration, the proportion of well-formed oriented vesicles also decreases with a corresponding increase in irregular shaped (collapsed) and coalesced voids (Fig. 18D, F).

Selected major element compositions (weight percent SiO_2 *vs.* $Na_2O + K_2O$ and FeO *vs.* K *vs.* $K_2O + CaO$) of glass shards from Lepué Tephra correlatives are presented in Fig. 19A–C. Two glass shard types can be clearly distinguished by differences in the major element analyses, namely (i) the rhyolitic composition of glass from the microlite-poor shards and (ii) the broadly basaltic–andesite composition of the intensely microlitic shards, which represent analyses of mixed glass and phenocrysts, approximating to a 'bulk' (modal) analysis of the glass shard, and not the glass phase only (cf. Platz *et al.*, 2007). The insets to Fig. 19 show the tight compositional clustering of rhyolitic glass shards erupted at the onset of the Lepué eruption and these probably represent the initial magma withdrawal from the top of a melt body dominated by fractionated magma (~71wt% SiO_2). Note that the rhyolitic end-member composition of Lepué Tephra can be clearly differentiated from all post-18 000 cal a BP rhyolitic tephra sourced from V. Chaitén-sourced tephra (indicated in grayscale).

Copyright © 2017 John Wiley & Sons, Ltd.

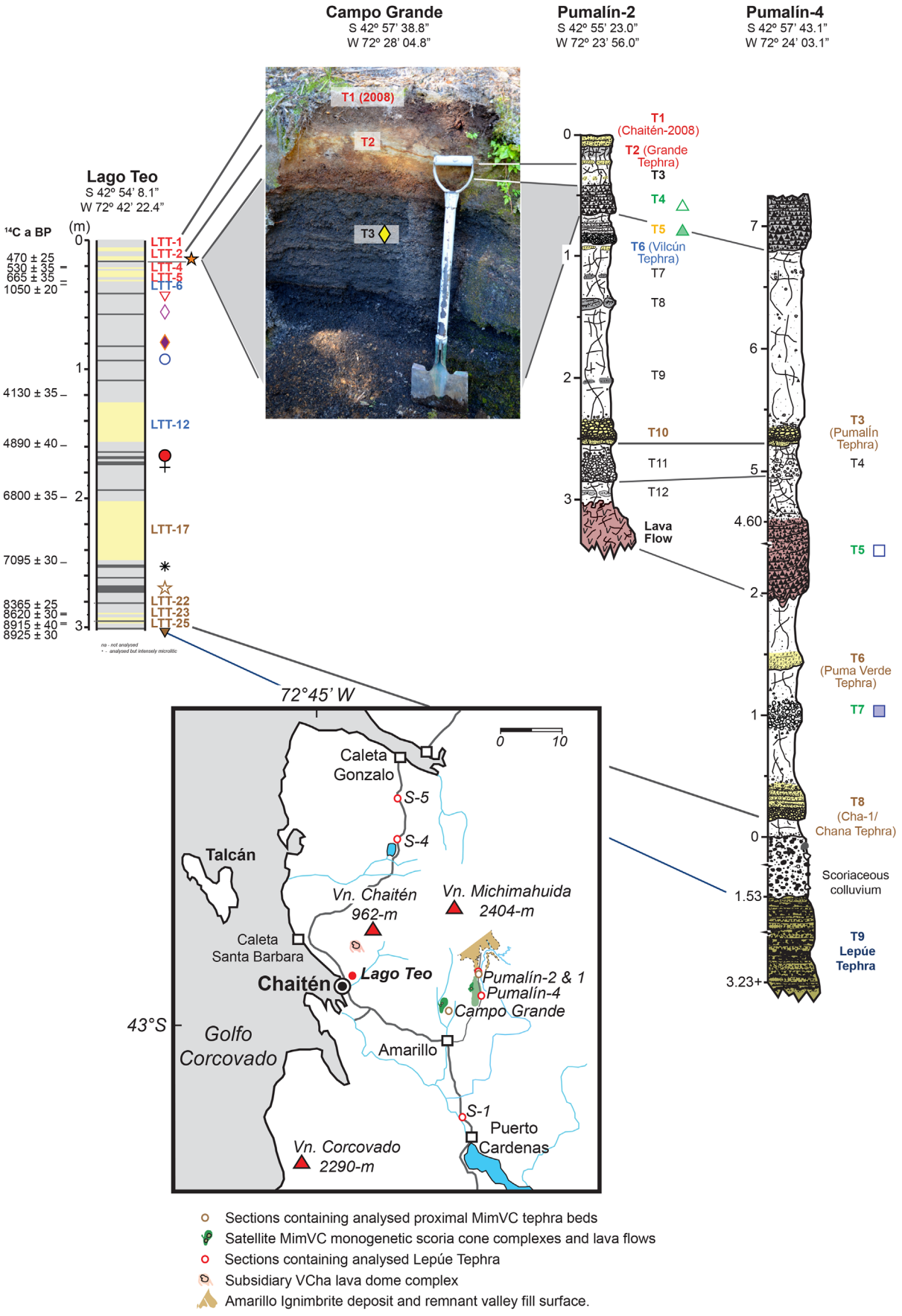

Figure 22. Sections containing analysed proximal tephra beds sourced from satellite MimVC monogenetic scoria cones. Inset map shows the location of associated satellite MimVC monogenetic scoria cone complexes and lava flows, sections containing analysed Lepué Tephra and Amarillo Ignimbrite and its remnant valley-fill surface.

Copyright © 2017 John Wiley & Sons, Ltd.

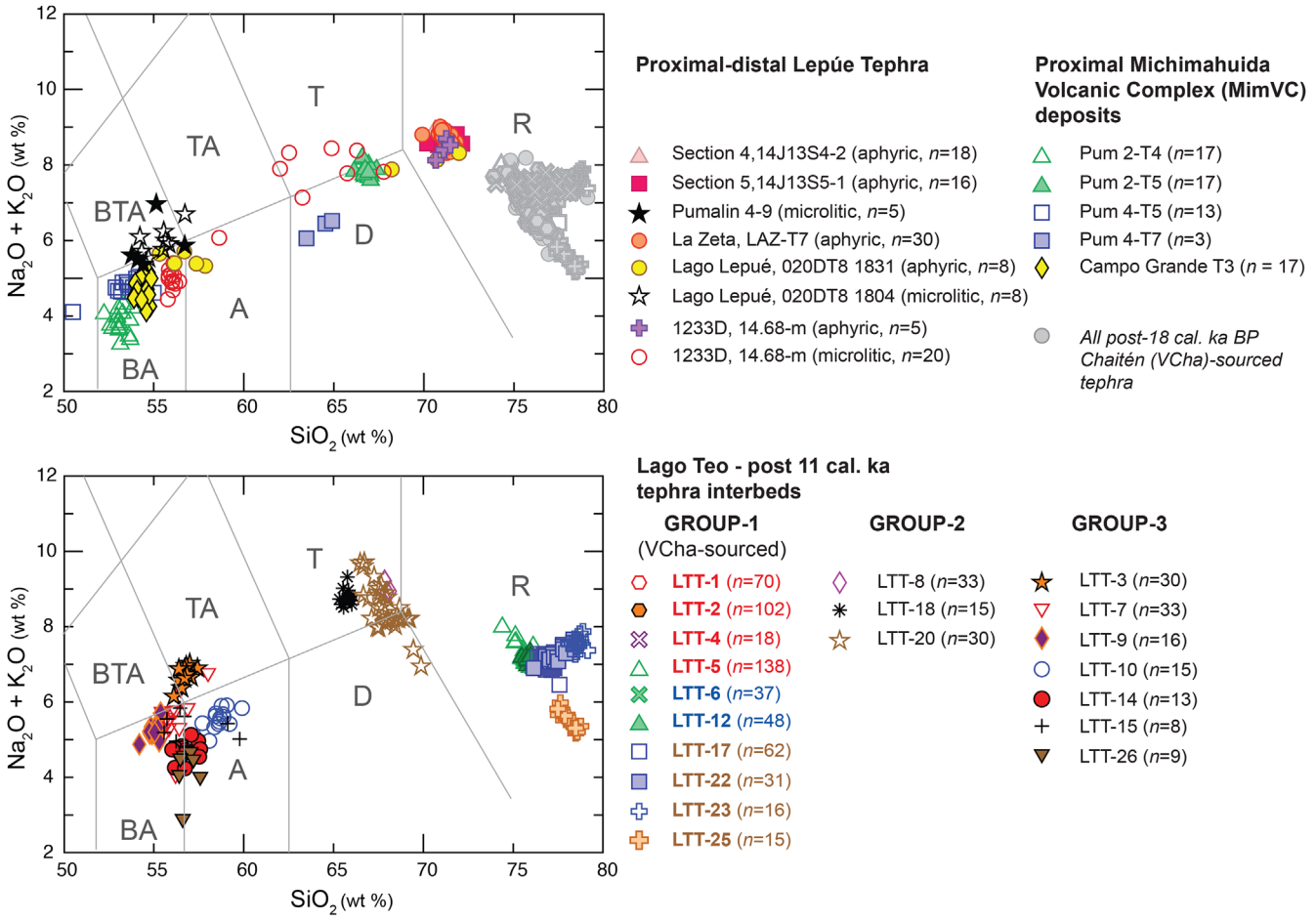

Figure 23. SiO_2 *vs.* $Na_2O + K_2O$ (wt%) compositions of glass shards from (A) proximal–distal Lepué Tephra compared with proximal tephra beds sourced from satellite MimVC monogenetic scoria cones, and (B) post-11 000 cal a BP tephra beds from L. Teo (Moreno *et al.*, 2015a). All tephra beds (except Pum 4-T7) as well as Group 2 and 3 tephra inter-beds from L. Teo occur on the same fractional crystallization pathway as analysed Lepué Tephra. The compositions of all post-18 000 cal a BP Chaitén-sourced tephra are indicated for comparison.

Selected trace element (Nd *vs.* Th and Sr *vs.* Y, Ho, Nd, Zr) compositions of glass shards from Lepué Tephra correlatives as determined by grain discrete LA-ICP-MS analyses are presented in Fig. 20. Data for glass shards from proximal sites at La Zeta, Puente Águila (S5) and Paso Lago Blanco (S4) sites are broadly coincident, showing strong linear relationships between the data in all plots. Samples from the more distal locations of Lago Lepué (020DT8, 1804 cm) and ODP-1233D (14.68 mcd) plot slightly away from the trend displayed in the other Lepué samples, but the low Sr endpoint of this compositional array is coincident, and the differences result from issues associated with the volume of material sampled during LA-ICP-MS microanalysis of microcryst-bearing glass shards.

All data display a range of compositions ranging from pure rhyolitic glass with a composition of ~ 72–113-p.p.m. Sr (i.e. microlite-free analyses from microlite-poor glass shards) to high Sr compositions (~1000-p.p.m. Sr) where the glasses become increasingly microlite-rich, with the highest Sr compositions coming from analyses which will have ablated almost entirely feldspar, with very little glass in the intensely microlitic shards. With increasing Sr, incompatible element concentrations decrease, associated with low incompatible element concentrations in feldspar. All analyses were calculated using the glass SiO_2 composition from the shards (determined by EPMA) as the internal standard (I.S.). This will give accurate analyses for the pure glass component (i.e. low Sr analyses), but the change in glass composition by inclusion of feldspar in the analyses will mean that, as more feldspar is ablated, the true SiO_2 content of the ablated mixture (the I.S. composition) moves further from the pure glass composition and the analyses will become progressively less accurate (see Pearce, 2014). Incorporation of plagioclase in rhyolitic glass causes the SiO_2 content in the ablated mixture to drop, and thus using the glass SiO_2 composition as I.S., analysed elements are marginally overestimated. It is not possible to correct the internal standard concentration for this effect unless the amount of feldspar ablated with glass and the SiO_2 composition of feldspar and glass are both accurately known. The effect of ablation of feldspar increases the reported Sr (compatible in feldspar) considerably and decreases incompatible element concentrations (by dilution, as feldspar has very low incompatible element contents), and this dilution effect competes with the increase in concentration from the change in I.S. composition, with the overall effect depending strongly on exactly how much phenocryst has been ablated (see Pearce, 2014); however without knowing its composition, the amount cannot be calculated. The offset of the Sr-rich analyses of microcryst-bearing glasses from the distal sites at Lago Lepué and ODP-1233D when compared with data from the more proximal sites may relate to differences in glass composition and phenocryst assemblage/content associated with deposition at different stages of the eruption, and the effects these variables may introduce into the LA-ICP-MS analyses described above. What is apparent though is that the microcryst-poor and microcryst-free glass analyses (i.e. where Sr < ~150-p.p.m.) from the more distal localities have the same glass composition as the microcryst-free glass analyses

Copyright © 2017 John Wiley & Sons, Ltd.

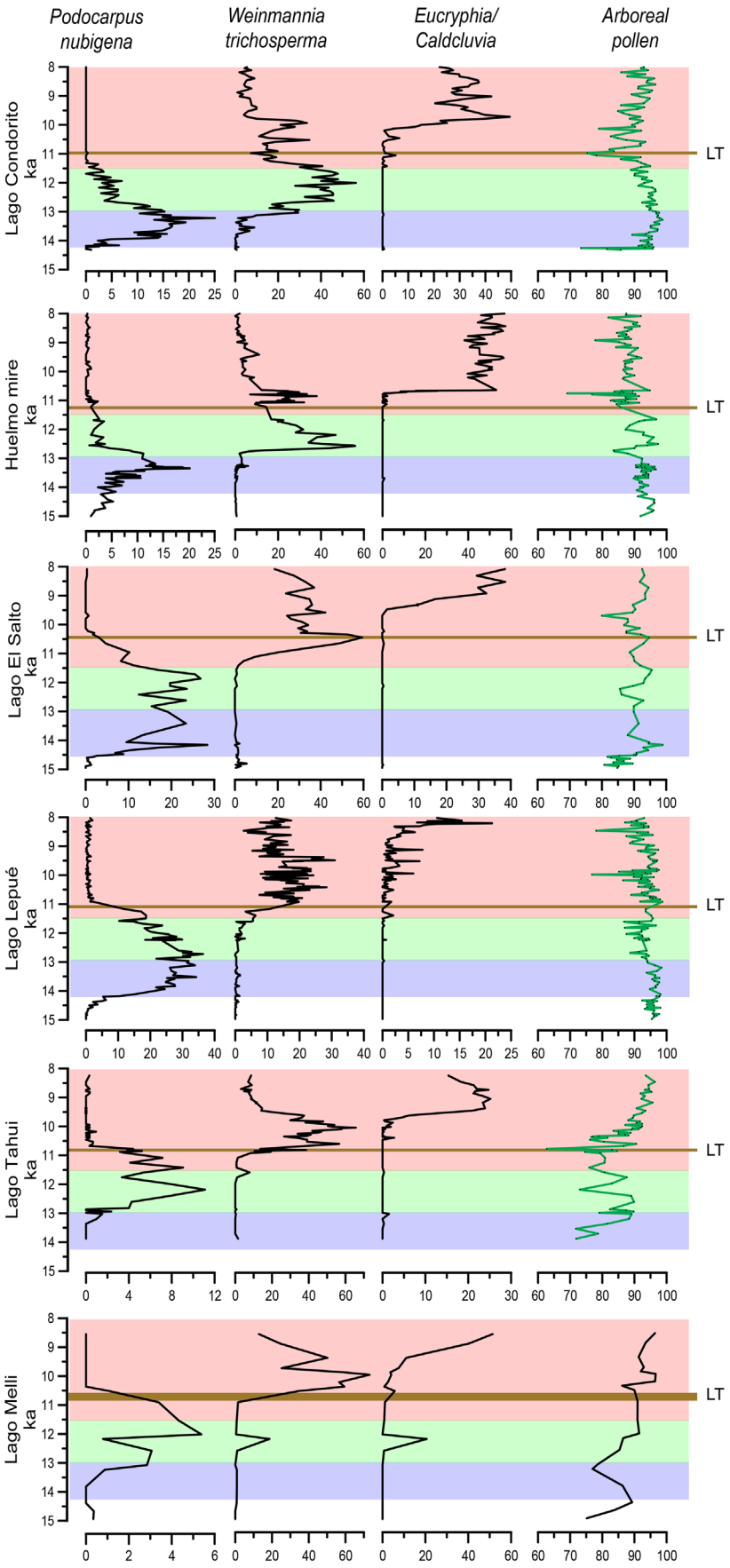

Figure 24. Pollen percentage curves of key taxa from six sites (arranged south to north; L. Melli, L. Tahui, L. Lepué, L. El Salto, Huelmo mire and L. Condorito; see Fig. 17) between 8000 and 15 000 cal a BP. Background blue represents an interval of interpreted cold/wet climate, green an interval of cold and seasonally dry climate, and pink an interval of warm and dry climate. Lepué Tephra occurs at all sites and its position within each record is indicated (LT).

Copyright © 2017 John Wiley & Sons, Ltd.

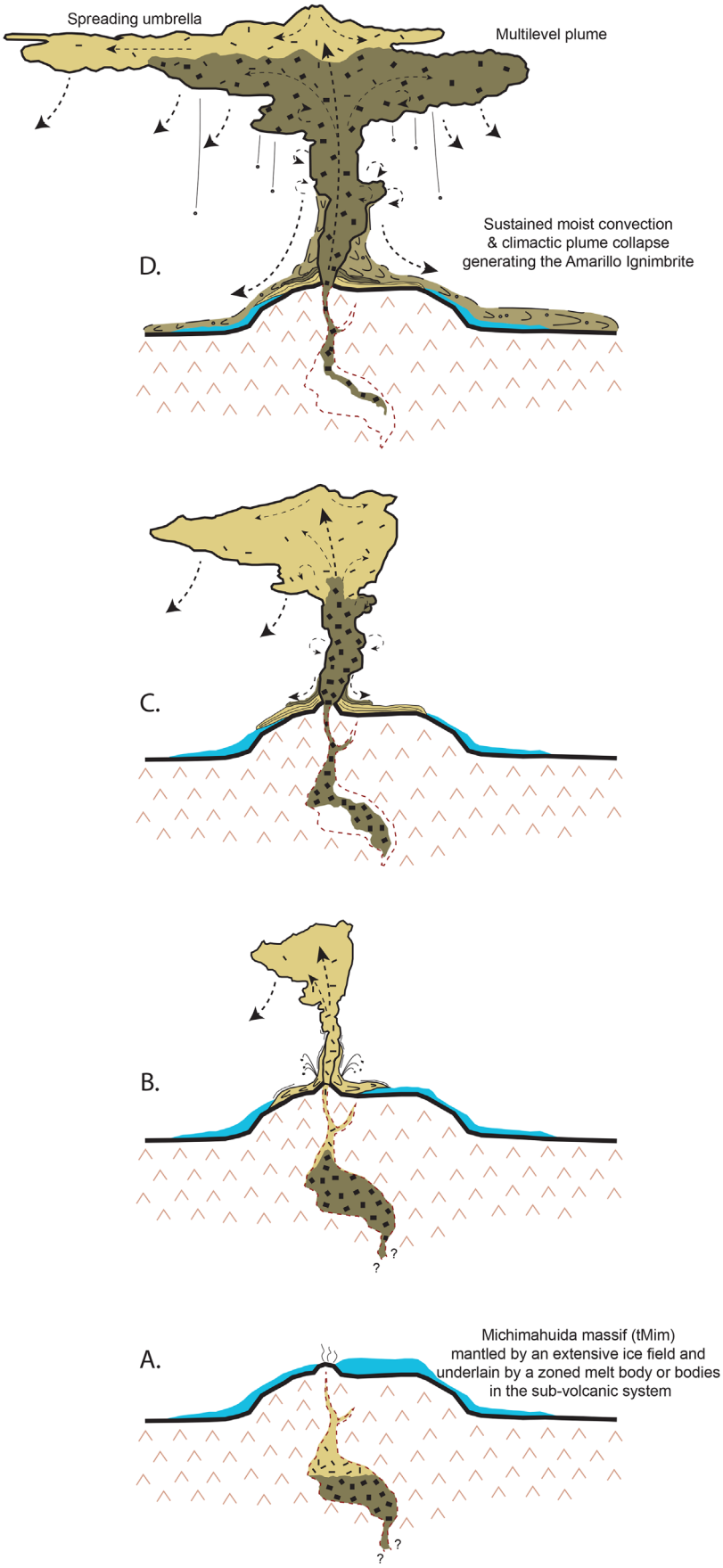

Figure 25. A schematic model for Lepué Tephra and its co-eruptive PDC (Amarillo Ignimbrite). (A) A zoned magma body within the MimVC sub-volcanic system comprising a volatile-rich cap of dominantly fractionated glass occurring on top of a more mafic phenocryst-rich magma. (B) Explosive phreatomagmatic eruption involving snow and ice from tMim and dominantly upward thrust of volatile-rich fractionated magma forming a stable column with associated fall dominated by aphyric glass; episodic moist convection generates flanking PDC deposits. (C) As the eruption continues, magma withdrawal steadily propagates downwards into the underlying crystal-rich magma and results in a fall increasingly dominated by microphenocrysts with very minor interstitial melt; intensified water vaporization results in heightened convection and plume instability. (D) Continued oscillations between buoyant (dry) and wet eruptive phases leads to the development of a multilevel plume; continued sustained moist convection and climactic plume collapse generates the Amarillo Ignimbrite.

Copyright © 2017 John Wiley & Sons, Ltd.

from the proximal localities, which establishes the correlation between these deposits (see Table S1) consistent with the well-constrained chronologies at these sites. This microcryst-free glass composition (Sr 73–113 p.p.m.) defines the composition (and compositional range) of the rhyolitic component of the Michimahuida magma at the onset of the eruption.

SN-ICP-MS analyses were also conducted on bulk ash material and individual accretionary lapilli from a number of proximal to distal sites (see Table S2). Plots of the highly immobile elements (i.e. Th *vs.* Zr) from Lepué Tephra correlatives from six proximal sites and 16 distal sites located on Isla Grande de Chiloé and the coastal Chilean mainland are presented in Fig. 21A. These results are compared with individually analysed accretionary lapilli from seven proximal Lepué Tephra localities (Fig. 21B). While bulk ash analyses exhibit a wide elemental range (even between duplicate samples) and predominantly along a tightly clustered linear fractional crystallization pathway, accretionary lapilli samples exhibit a narrower elemental range positioned on the same linear pathway as the bulk ash samples. Lepué analyses were compared with similar analyses from Holocene-aged tephra beds (13) of tMim and its adjacent monogenetic satellite cones (here named Michimahuida Volcanic Complex, MimVC) (Fig. 21C). The elemental spread and orientation of tephra points are coincident along the Lepué Tephra linear evolutionary trend. These results indicate the limited utility of bulk analyses in the absence of associated chronostratigraphic contexts to be able to adequately differentiate MimVC-sourced eruptives. Results also indicate that all MimVC-sourced tephras, irrespective of age, are fractionating under broadly similar phase equilibria constraints.

Confirming Michimahuida as the eruptive source

Glass shard major-element chemistry indicates that the initial eruptive phase of Lepué Tephra is rhyolitic in composition but distinguishable from all post-18 000 cal a BP Chaitén-sourced tephra. As the Lepué eruption progresses the composition steadily becomes more basic and terminates in a compositional field that broadly straddles the trachyte–andesite, andesite, basaltic–trachyte–andesite and basaltic–andesite fields (Fig. 19). This trend suggests a zoned magma body with a volatile-rich aphyric cap above a more mafic and phenocryst-rich magma. This more mafic end member of Lepué Tephra is similar to the composition (basaltic–andesite) of proximal MimVC deposits exposed at Campo Grande, Pumalín-2 and Pumalín-4 (Fig. 22). At these localities, dm-thick lapilli beds (CG-T3, Pum 2-T4, Pum 4-T5) can be directly associated with adjacent MimVC monogenetic scoria cone complexes and lava flows. Two coarse-grained pumiceous lapilli and ash beds (Pum 2-T5 and Pum 4-T7) have distinct compositions that straddle the trachyte and dacite fields and on the same compositional trend as MimVC-sourced tephra (Fig. 23). While these two tephra cannot be associated with an identifiable MimVC source vent, coarse grain size and thickening characteristics would tend to indicate a putative MimVC source. The three compositional groups identified from proximal MimVC sites are similar to those identified from L. Teo (Moreno *et al.*, 2015a) and indicate a diverse range of discrete small-volume silicic to mafic melt bodies resident at different levels within the MimVC sub-volcanic system and may reflect contributions from different upper mantle components (i.e. Hickey *et al.*, 1986; Hickey-Vargas *et al.*, 2002), differences in rates of crustal stagnation and differentiation as well as structural controls (i.e. López-Escobar *et al.*, 1995).

Discussion

Relationship of Lepué Tephra to deglaciation

Lepué Tephra is one of the most widespread tephra marker beds to occur in this sector in the last 11 000 years and its early Holocene age is ideal for assessing the timing and rate of deglaciation and associated environmental changes as the climate ameliorated at the transition between the LGM and early Holocene.

Radiocarbon dates of organic material retrieved from the base of cores and sections through lacustrine and organic-rich sediments that overlie glacial deposits situated in areas formerly covered by ice lobes have been pivotal in terms of assessing the temporal–spatial extent of glaciers in this region and, of relevance to this study, the timing of rapid ice lobe recession that followed the LGT advance into the LGM moraine belt. For example, a basal radiocarbon date from a low-elevation stratigraphic section containing Lepué Tephra at Puelche (Fig. 5) indicates a minimum-limiting age of 14 070 ± 35 ^{14}C a BP (17 107 ± 99 cal a BP) for recession of the Seno Reloncaví ice lobe. Similarly, a radiocarbon date from a coastal roadside outcrop just north of Chaitén (Section 12A, Fig. 2) (also containing Lepué Tephra) indicates a minimum-limiting age of 13 830 ± 50 ^{14}C a BP (16 737 ± 125 cal a BP) for recession of the Golfo de Corcovado ice lobe. The persistence of ice lobes within low-elevation Cordilleran valley sites is indicated from minimum ages of *c.* 12 500 ^{14}C a BP (14 600 cal a BP) from basal organic mud sequences overlying glacial till (i.e. Sta. Lucía, Fig. 7). Certainly, the spatial range of dates presented in this study supports the findings of Moreno *et al.* (2015b) that wholesale glacial recession in this region following the final advance of Andean ice lobes during a cold and wet LGT episode (17 700–18 100 cal a BP) was very abrupt with diminished lobes recessed within the confines of continental Andean valleys in <1000 years.

Synchronization of late last glacial to early post-glacial vegetation and climate records

Pollen percentage curves of selected key taxa from six sites (arranged south to north; L. Melli, L. Tahui, L. Lepué, L. El Salto, Huelmo mire and L. Condorito) between 8000 and 15 000 cal a BP are shown in Fig. 24. While sediment cores from these sites have been individually described in the literature, the recognition of the widespread Lepué Tephra within these cores enables us to effectively time-slice and synchronize vegetation/climate records across a broad latitudinal swath of north-western Patagonia and west of the Cordillera de los Andes. An intraregional summary of these synchronized records is presented here.

Palynological studies of organic sediments from numerous lake cores and cover-bed sections that overlie glacial deposits or bedrock situated in areas formerly covered by ice lobes indicate that the interval preceding Lepué Tephra (11 700–15 000 cal a BP) features a dominance of closed-canopy temperate rainforests. Palynological records from lowland sites indicate a prominent increase in the cold-resistant conifer *Podocarpus nubigena* starting at ~14 500 cal a BP, concomitant with a decline in thermophilous rainforest trees (Myrtaceae) and vines (Hydrangea) (Moreno, 1997, 2004; Moreno *et al.*, 1999, 2001; Moreno and León, 2003). The species *P. nubigena* attained its maximum abundance between 12 700 and 13 000 cal a BP, declined between 11 000 and 12 700 cal a BP and then reached minimum abundance until 8000 cal a BP These changes suggest a cooling trend and increase in precipitation between ~12 700 and

Copyright © 2017 John Wiley & Sons, Ltd.

14 500 cal a BP, followed by a decline in precipitation and/or enhanced precipitation seasonality with intense fire activity between ~11 000 and 12 700 cal a BP. Mainland sites show that fire disturbance promoted forest gaps and colonization of the opportunistic, shade-intolerant tree *Weinmannia trichosperma* over a cold and highly variable interval between ~11 000 and 12 700 cal a BP. Over the same interval, sites in Isla Grande de Chiloé (Abarzúa *et al.*, 2004; Abarzúa and Moreno, 2008; Pesce and Moreno, 2014) show diversification of the forest canopy, lake-level lowering and encroachment of species of the myrtle family along the lake periphery. Deposition of the Lepué Tephra at ~11 000 cal a BP occurred when *P. nubigena* had already reached low abundance in mainland palynological sites (L. Condorito, Huelmo mire), and at the culmination of a rapid decline of this conifer in Chilotan sites (L. Lepué, L. Melli, L. Tahui). Chilotan sites show abrupt increases in *W. trichosperma* following deposition of the Lepué Tephra; likewise, mainland sites exhibit a secondary expansion of this species. These changes have been interpreted as changes in temperature and precipitation, the latter associated with variation in intensity in the southern westerly winds (SWWs) attributable to latitudinal shifts or intensity variations. Recent studies (Moreno *et al.*, 2010, 2012, 2015b) have proposed that the SWWs intensified during the Antarctic Cold Reversal (~12 700–14 500 cal a BP), shifted pole-ward during the Younger Dryas (~11 500–12 700 cal a BP) and then weakened during the early Holocene (~7800–11 500 cal a BP). These changes covaried with temperature and paleofires, with warm/dry conditions featuring enhanced fire activity and cold/wet climates inhibiting paleofires. Deposition of the Lepué Tephra occurred at the beginning of the warmest/driest interval of the last glacial–interglacial cycle, when the SWWs attained their weakest condition and when SSTs from core ODP-1233 reach a maximum of 15.6 °C in the early Holocene (11 000–9000 cal a BP) (Kaiser *et al.*, 2005, 2008; Heusser *et al.*, 2006).

Prevailing warm/dry climate conditions coupled with weak SWW flow might account for the broad distribution of Lepué Tephra west of Volcán Michimahuida at a time when zonal atmospheric flow did not impede its northwestward distribution towards the SE Pacific. However, the distribution of Lepué Tephra may have also been influenced by volcanological factors, in particular a hybrid dry/wet plume that expands outward as a powerfully spreading umbrella cloud (see section below).

Eruption style and hazard implications

A schematic representation of the Lepué eruptive sequence centered at tMim is represented in Fig. 25. Dark gray, poorly sorted, fine-grained subunits of Lepué Tephra with accretionary lapilli and rain-flushed pore spaces within the ashy matrix clearly indicate the involvement of external water within the erupted mixture. The eruption comprising Lepué Tephra and its co-eruptive PDC (Amarillo Ignimbrite) is an excellent example of an early Holocene dominantly phreatomagmatic eruption derived from a volcanic massif presently mantled by an extensive area of permanent ice. Such eruptions are less usual than the more typical background of Strombolian to Plinian volcanism frequently experienced in this region during the Holocene. Thus, in the absence of proximal exposures on Volcán Michimahuida, it is not known if Lepué eruption was point-sourced and derived from a single magma reservoir, or derived from a network of coalescing and/or discrete multiple co-genetic melt bodies (i.e. similar to the 2011 Puyehue–Cordón Caulle eruption, see Alloway *et al.*, 2015).

Within most sections adjacent to tMim, meter-thick accretionary lapilli bearing ash deposits with weak stratification between coarser and finer components can be observed and indicate fluctuating multilevel deposition; that is, coarse ash and lapilli transported farther during stable phases of the eruption (less water content with higher vertical velocities), yet deposited closer to source during periods of unstable water-rich plumes where moist convection simultaneously occurs both vertically and laterally away from the vent. If moist convection was a dominant feature of the Lepué plume, then a substantial portion of the initially erupted mass was probably ejected and maintained in the troposphere where temperature inversions inhibit the rise of the weaker, less stable portions of the eruption column. Under such circumstances, the ash plume would have had the tendency to spread outward as a broad, umbrella-shaped cloud. The combination of fluctuating multilevel transport/deposition and upwind/cross wind expansion at the troposphere would probably have favored the formation of a radially symmetrical ash cloud (see Houghton *et al.*, 2015). Indeed, recorded thicknesses of Lepué Tephra over such an extensive area in all directions from source appear to support this scenario (Fig. 17). While eruptive conditions were probably conducive to the broad radial distribution noted for Lepué Tephra, this distribution could also be attributed to the reduced SWW intensity interpreted from equivalent-aged environmental records.

In the advent of a future sustained eruption of similar magnitude to the Lepué eruption centered upon the ice-capped tMim, a cm-thick wet ash fall could be reasonably expected up to ~200 km from the volcanic source, potentially affecting communities and critical infrastructure westward in Isla Grande de Chiloé, northwards towards the city of Puerto Montt and east and south-eastwards towards the communities of Futaleufú on the Chilean frontier and Esquel and Trevelin located in Argentina. Eruption-induced sub-glacial and surface melting of ice and snow on tMim is also likely to occur and lead to significant meltwater formation, jökulhlaups and lahars extending down adjacent tributaries. Such events have already been shown to be a significant hazard in areas of Iceland (i.e. Katla in 1918, Eyjafjallajökull in 2010), Alaska (i.e. Redoubt in 2009), Cascades (i.e. Mt Rainier), Antarctica (i.e. Deception Island in 1969) and in parts of the Andes (i.e. Nevado del Ruiz in 1985). Although the area surrounding Volcán Michimahuida is sparsely populated with little critical infrastructure, meltwater floods and/or water-supported mass-flows would inundate picturesque and increasingly popular low-lying riverside tourist campgrounds within Parque Pumalín and scattered farm dwellings farther downstream. The community of Amarillo would probably be affected, although inundation is likely to be minimized by recent engineering works that have elevated and armored adjacent river banks.

In summary, while Lepué Tephra is temporally associated with rhyolitic products from nearby Volcan Chaitén, it has physical and geochemical attributes typical of a complex (zoned) phreatomagmatic eruption sourced from tMim. We propose that the eruption commenced with initial magma withdrawal from the top of a melt body dominated by fractionated Si-rich magma (~71wt% SiO_2), which propagated downwards into the hosting crystalline-rich magma and ultimately resulted in the Si-rich magma being rapidly and almost entirely replaced by microphenocrysts with very minor interstitial melt (~55wt% bulk SiO_2). Despite compositional heterogeneity, we were still able to characterize both the aphyric and the microlitic glass of the Lepué Tephra by grain discrete and bulk analytical techniques to define a broad compositional array enabling us to distinguish and widely

Copyright © 2017 John Wiley & Sons, Ltd.

correlate this tephra marker in both terrestrial and marine realms of north-western Patagonia. While discrete and bulk glass shard trace element analyses may be of significant use in petrogenetic studies, this study also illustrates its utility in substantiating correlation beyond that already established from major element (EMP) analyses.

Lepué Tephra with its phreatomagmatic style and its compositional heterogeneity is exceptional in the context of other documented eruptions known from this Andean sector. We consider that our integrative approach of intensive mapping supported by multi-technique geochemical analysis is a useful template for the characterization and correlation of such complex and compositionally variable tephra deposits elsewhere. Ultimately, our approach applied to weathered tephra in wet, hyper-humid environments, like that of north-western Patagonia, will be of great assistance in the synchronization of different equivalent-aged sedimentary archives.

Acknowledgements. This study was funded by Iniciativa Científica *Milenio* grants P02-51 and NC120066, Fondecyt 1151469 (to P.I.M.), part funded by a Victoria University of Wellington Science Faculty Research Grant (to B.V.A.), Aberystwyth University Research Fund (to N.J.G.P.), Fondecyt 1160488 (to E.S.) and PIP CONICET 2011 0311 (to G.V.). Andy Brown (IGES, Aberystwyth University, UK) is thanked for conducting solution-ICP-MS acid digestions and Craig Wickham for conducting acid digestions and solution-ICP-MS analyses on Lepué Tephra accretionary lapilli (under supervision by N.J.G.P.). Ignacio Jara, Rodrigo Ras and Craig Wickham are thanked for their assistance in the field and Matt Ryan for his statistical analysis of radiocarbon dates. We are grateful to Frank Lamy and Thomas Ronge (Alfred Wegener Institute, Bremerhaven, Germany) for tephra samples and data from ODP Site 1233. We extend our appreciation to Horacio Griffero and Gabriela Piezug of Posada Kahuel (km-4 Camino Chaitén-Santa Bárbara; www.posadakahuel.cl) for their continuing hospitality and friendship while engaging in fieldwork. Our sincere thanks go to the residents of Chaitén township for their hospitality, as well as unwavering curiosity and support of this research. P. A. Shane and an anonymous reviewer are thanked for their comments. The authors also wish to thank Andrew Lorrey for his editorial input.

Supporting information

Geochemical methods associated with the acquisition of major- and trace-element analyses from Lepue Tephra.

Table S1. Summary of individual glass shard trace element compositions of proximal to distal Lepué Tephra in the Chaitén, Isla Grande de Chiloé and Esquel sectors of NW Patagonia obtained by LA-ICP-MS at Aberystwyth. All concentrations in parts per million unless otherwise stated.

Table S2. All trace element concentrations from bulk Lepué Tephra correlative samples obtained by SN-ICP-MS at Aberystwyth University, Wales. All concentrations in parts per million unless otherwise stated.

Abbreviations. ACC, Antarctic Circumpolar Current; BSE, back-scatter electron; EPMA, electron microprobe analysis; I.S., internal standard; LA-ICP-MS, laser ablation inductively coupled plasma-mass spectrometry; LGM, Last Glacial Maximum; LGT, Last Glacial Termination; mcd, meters composite depth; MimVC, Michimahuida Volcanic Complex; MIS, Marine Isotope Stage; PCC, Perú–Chile current; PDC, pyroclastic density current; SN-ICP-MS, solution nebulization inductively coupled plasma mass spectrometry; SVZ, Southern Volcanic Zone; SWWs, southern westerly winds; tMim, Volcán Michimahuida massif; VCha, Volcán Chaitén.

References

Abarzúa AM, Moreno PI. 2008. Changing fire regimes in the temperate rainforest region of southern Chile over the last 16,000 yr. *Quaternary Research* **69**: 62–71.

Abarzúa AM, Villagrán C, Moreno PI. 2004. Deglacial and postglacial climate history in east-central Isla Grande de Chiloé, southern Chile (43°S). *Quaternary Research* **62**: 49–59.

Alloway BV, Pearce NJ, Villarosa G *et al.* 2015. Multiple melt bodies fed the AD 2011 eruption of Puyehue-Cordón Caulle, Chile. *Scientific Reports* **5**: 17589.

Alloway BV, Pearce NJG, Moreno PI *et al.* 2017. An 18,000 year-long eruptive record from Volcán Chaitén, northwestern Patagonia: paleoenvironmental and hazard-assessment implications. *Quaternary Science Reviews* **168**: 151–181.

Amigo A, Lara LE, Smith VC. 2013. Holocene record of large explosive eruptions from Chaitén and Michimahuida Volcanoes, Chile. *Andean Geology* **40**: 227–248.

Andersen B, Denton GH, Lowell TV. 1999. Glacial geomorphologic maps of Llanquihue Drift in the area of the Southern Lake District, Chile. *Geografiska Annaler, Series A: Physical Geography* **81**: 155–166.

Bertrand S, Charlet F, Charlier B *et al.* 2008. Climate variability of southern Chile since the Last Glacial maximum: a continuous sedimentological record from Lago Puyehue (40°S). *Journal of Paleolimnology* **39**: 179–195.

Cas RAF, Wright JV. 1987. *Volcanic Successions, Modern and Ancient*. Chapman & Hall: London.

Daga R, Guevara SR, Sánchez ML *et al.* 2010. Tephrochronology of recent events in the Andean Range (northern Patagonia): spatial distribution and provenance of lacustrine ash layers in the Nahuel Huapi National Park. *Journal of Quaternary Science* **25**: 1113–1123.

Denton GH, Lowell TV, Heusser CJ *et al.* 1999. Geomorphology, stratigraphy and radiocarbon chronology of Llanquihue drift in the area of the Southern Lake District, Seno Relongcaví and Isla Grande de Chiloé, Chile. *Geografiska Annaler, Series A: Physical Geography* **81B**: 167–229.

Fisher RV, Schmincke H-U. 1984. *Pyroclastic Rocks*. Springer-Verlag: Berlin.

Fontijn K, Lachowycz SM, Rawson H *et al.* 2014. Late Quaternary tephrostratigraphy of southern Chile and Argentina. *Quaternary Science Reviews* **89**: 70–84.

Fontijn K, Rawson H, Van Daele M *et al.* 2016. Synchronisation of sedimentary records using tephra: a postglacial tephrochronological model for the Chilean Lake District. *Quaternary Science Reviews* **137**: 234–254.

Haberle SG, Lumley SH. 1998. Age and origin of tephras recorded in postglacial lake sediments to the west of the southern Andes, 44°S to 47°S. *Journal of Volcanology and Geothermal Research* **84**: 239–256.

Henríquez WI, Moreno PI, Alloway BV *et al.* 2015. Vegetation and climate change, fire-regime shifts and volcanic disturbance in Chiloé Continental (43°S) during the last 10,000 years. *Quaternary Science Reviews* **123**: 158–167.

Heusser CJ, Heusser LE. 2006. Submillenial palynology and palaeoecology of the last glaciation at Taiquemo (50,000 cal. yr, MIS 2–4) in southern Chile. *Quaternary Science Reviews* **25**: 446–454.

Heusser L, Heusser C, Pisias N. 2006. Vegetation and climate dynamics of southern Chile during the past 50,000 years: results of ODP Site 1233 pollen analysis. *Quaternary Science Reviews* **25**: 474–485.

Hickey RL, Frey FA, Gerlach DC *et al.* 1986. Multiple sources for basaltic arc rocks from the southern volcanic zone of the Andes (34°–41°S): Trace element and isotopic evidence for contributions from subducted oceanic crust, mantle, and continental crust. *Journal of Geophysical Research* **91**: 5963–5983.

Hickey-Vargas R, Sun M, López-Escobar L *et al.* 2002. Multiple subduction components in the mantle wedge: Evidence from eruptive centers in the Central Southern volcanic zone, Chile. *Geology* **30**: 199–202.

Houghton B, White JDL, Van Eaton AR. 2015. Phreatomagmatic and related eruption styles. In *The Encyclopedia of Volcanoes*, Sigurdsson H (ed.). Academic Press: San Diego; 537–552.

Iglesias V, Whitlock C, Bianchi MM *et al.* 2012. Holocene climate variability and environmental history at the Patagonian forest/steppe ecotone: Lago Mosquito (42°29′37.89″S, 71°24′14.57″W) and Laguna del Cóndor (42°20′47.22″S, 71°17′07.62″W). *The Holocene* **22**: 1297–1307.

Copyright © 2017 John Wiley & Sons, Ltd.

Kaiser J, Lamy F, Hebbeln D. 2005. A 70-kyr sea surface temperature record off southern Chile (Ocean Drilling Program Site 1233). *Paleoceanography* **20**: PA4009.

Kaiser J, Schefuß E, Lamy F *et al.* 2008. Glacial to Holocene changes in sea surface temperature and coastal vegetation in north central Chile: high versus low latitude forcing. *Quaternary Science Reviews* **27**: 2064–2075.

Lamy F, Kaiser J, Arz HW *et al.* 2007. Modulation of the bipolar seesaw in the Southeast Pacific during Termination 1. *Earth and Planetary Science Letters* **259**: 400–413.

Lara LE. 2009. The 2008 eruption of the Chaitén Volcano, Chile: A preliminary report. *Andean Geology* **36**: 125–129.

Lara LE, Moreno H, Naranjo JA *et al.* 2006. Magmatic evolution of the Puyehue–Cordón Caulle Volcanic Complex (40° S), Southern Andean Volcanic Zone: From shield to unusual rhyolitic fissure volcanism. *Journal of Volcanology and Geothermal Research* **157**: 343–366.

Lara LE, Moreno R, Amigo Á *et al.* 2013. Late Holocene history of Chaitén Volcano: new evidence for a 17th century eruption. *Andean Geology* **40**: 249–261.

López-Escobar L, Kempton PD, Moreno H *et al.* 1995. Calbuco volcano and minor eruptive centers distributed along the Liquine-Ofqui fault zone, Chile (41°–42°S): contrasting origin of andesitic and basaltic magma in the Southern Volcanic Zone of the Andes. *Contributions to Mineralogy and Petrology* **119**: 345–361.

Mercer JH. 1976. Glacial history of Southernmost South America. *Quaternary Research* **6**: 125–166.

Moreno PI. 1997. Vegetation and climate near Lago Llanquihue in the Chilean Lake District between 20200 and 9500 C-14 yr BP. *Journal of Quaternary Science* **12**: 485–500.

Moreno PI. 2004. Millennial-scale climate variability in northwest Patagonia over the last 15000 yr. *Journal of Quaternary Science* **19**: 35–47.

Moreno PI, Alloway BV, Villarosa G *et al.* 2015a. A past-millennium maximum in postglacial activity from Volcan Chaiten, southern Chile. *Geology* **43**: 47–50.

Moreno PI, Denton GH, Moreno H *et al.* 2015b. Radiocarbon chronology of the last glacial maximum and its termination in northwestern Patagonia. *Quaternary Science Reviews* **122**: 233–249.

Moreno PI, Francois JP, Moy CM *et al.* 2010. Covariability of the Southern Westerlies and atmospheric CO_2 during the Holocene. *Geology* **38**: 727–730.

Moreno PI, Jacobson GL, Andersen BG *et al.* 1999. Abrupt vegetation and climate changes during the last glacial maximum and the last Termination in the Chilean Lake District: a case study from Canal de la Puntilla (41°S). *Geografiska Annaler, Series A: Physical Geography* **81A**: 285–311.

Moreno PI, Jacobson GL, Lowell TV *et al.* 2001. Interhemispheric climate links revealed by late-glacial cooling episode in southern Chile. *Nature* **409**: 804–808.

Moreno PI, León AL. 2003. Abrupt vegetation changes during the last glacial to Holocene transition in mid-latitude South America. *Journal of Quaternary Science* **18**: 787–800.

Moreno PI, Videla J. 2016. Centennial and millennial-scale hydroclimate changes in northwestern Patagonia since 16,000 yr BP. *Quaternary Science Reviews* **149**: 326–337.

Moreno PI, Villa-Martínez R, Cárdenas ML *et al.* 2012. Deglacial changes of the southern margin of the southern westerly winds revealed by terrestrial records from SW Patagonia (52°S). *Quaternary Science Reviews* **41**: 1–21.

Naranjo JA, Singer BS, Jicha BR *et al.* 2017. Holocene tephra succession of Puyehue-Cordón Caulle and Antillanca/Casablanca volcanic complexes, southern Andes (40–41°S). *Journal of Volcanology and Geothermal Research* **332**: 109–128.

Naranjo JA, Stern CR. 2004. Holocene tephrochronology of the southernmost part (42°30′–45°S) of the Andean Southern Volcanic Zone. *Revista Geológica de Chile* **31**: 225–240.

Ngwa CN, Suh CE, Devey CW. 2010. Phreatomagmatic deposits and stratigraphic reconstruction at Debunscha Maar (Mt Cameroon volcano). *Journal of Volcanology and Geothermal Research* **192**: 201–211.

Ort MH, Carrasco-Núñez G. 2009. Lateral vent migration during phreatomagmatic and magmatic eruptions at Tecuitlapa Maar, east-central Mexico. *Journal of Volcanology and Geothermal Research* **181**: 67–77.

Pearce NJG. 2014. Towards a protocol for the trace element analysis of glass from rhyolitic shards in tephra deposits by laser ablation ICP-MS. *Journal of Quaternary Science* **29**: 627–640.

Pesce OH, Moreno PI. 2014. Vegetation, fire and climate change in central-east Isla Grande de Chiloé (43°S) since the Last Glacial Maximum, northwestern Patagonia. *Quaternary Science Reviews* **90**: 143–157.

Platz T, Cronin SJ, Smith IEM et al. 2007. Improving the reliability of microprobe-based analyses of andesitic glasses for tephra correlation. *The Holocene* **17**: 573–583.

Rawson H, Naranjo JA, Smith VC *et al.* 2015. The frequency and magnitude of post-glacial explosive eruptions at Volcán Mocho-Choshuenco, southern Chile. *Journal of Volcanology and Geothermal Research* **299**: 103–129.

Singer BS, Jicha BR, Harper MA *et al.* 2008. Eruptive history, geochronology, and magmatic evolution of the Puyehue-Cordón Caulle volcanic complex, Chile. *Geological Society of America Bulletin* **120**: 599–618.

Stern CR. 2004. Active Andean volcanism: its geologic and tectonic setting. *Revista Geológica de Chile* **31**: 161–206.

Stern CR. 2008. Holocene tephrochronology record of large explosive eruptions in the southernmost Patagonian Andes. *Bulletin of Volcanology* **70**: 435–454.

Stern CR, Moreno H, Lopez-Escobar L *et al.* 2007. Chilean volcanoes. In *The Geology of Chile*, Moreno T, Gibbons W (eds). Geological Society: London; 147–178.

van Otterloo J, Cas RAF. 2016. Low-temperature emplacement of phreatomagmatic pyroclastic flow deposits at the monogenetic Mt Gambier Volcanic Complex, South Australia, and their relevance for understanding some deposits in diatremes. *Journal of the Geological Society* **173**: 701–710.

Watt SFL, Pyle DM, Mather TA. 2013. Evidence of mid- to late-Holocene explosive rhyolitic eruptions from Chaitén Volcano, Chile. *Andean Geology* **40**: 216–226.

Watt SFL, Pyle DM, Naranjo JA *et al.* 2011. Holocene tephrochronology of the Hualaihue region (Andean southern volcanic zone, ~42°S), southern Chile. *Quaternary International* **246**: 324–343.

Wilson TM, Cole JW, Cronin SJ *et al.* 2011a. Impacts on agriculture following the 1991 eruption of Volcán Hudson, Patagonia: lessons for recovery. *Natural Hazards* **57**: 185–212.

Wilson TM, Cole JW, Stewart C *et al.* 2011b. Ash storms: impacts of wind-remobilised volcanic ash on rural communities and agriculture following the 1991 Hudson eruption, southern Patagonia, Chile. *Bulletin of Volcanology* **73**: 223–239.

Zimanowski B. 1998. Phreatomagmatic explosions. In *From Magma to Tephra: Developments in Volcanology 4*, Freundt A, Rosi M (eds). Elsevier: Amsterdam; 25–54.

Copyright © 2017 John Wiley & Sons, Ltd.